

1 **Preparation and characterization of multi-component tablets**
2 **containing co-amorphous salts: combining multimodal non-**
3 **linear optical imaging with established analytical methods**

4 Rami Ojarinta^{a,*}, Jukka Saarinen^b, Clare J. Strachan^b, Ossi Korhonen^a, Riikka Laitinen^a

5 ^a School of Pharmacy, University of Eastern Finland, P.O. Box 1627, 70211 Kuopio, Finland

6 ^b Drug Research Program, Division of Pharmaceutical Chemistry and Technology, Faculty of
7 Pharmacy, University of Helsinki, Viikinkaari 5 E, 00014 University of Helsinki, Finland

8

9

10

11

12

13

14

15

16

17 *Corresponding author:

18 Tel. +358 40 355 3870

19 E-mail: rami.ojarinta@uef.fi

20 **ABSTRACT**

21 Co-amorphous mixtures have rarely been formulated as oral dosage forms, even though they have
22 been shown to stabilize amorphous drugs in the solid state and enhance the dissolution properties of
23 poorly soluble drugs.

24 In the present study we formulated tablets consisting of either spray dried co-amorphous ibuprofen-
25 arginine or indomethacin-arginine, mannitol or xylitol and polyvinylpyrrolidone K30 (PVP).

26 Experimental design was used for the selection of tablet compositions, and the effect of tablet
27 composition on tablet characteristics was modelled. Multimodal non-linear imaging, including
28 coherent anti-Stokes Raman scattering (CARS) and sum frequency/second harmonic generation
29 (SFG/SHG) microscopies, as well as scanning electron microscopy, X-ray diffractometry and
30 Fourier-transform infrared spectroscopy were utilized to characterize the tablets.

31 The tablets possessed sufficient strength, but modelling produced no clear evidence about the
32 compaction characteristics of co-amorphous salts. However, co-amorphous drug-arginine mixtures
33 resulted in enhanced dissolution behaviour, and the PVP in the tableting mixture stabilized the
34 supersaturation. The co-amorphous mixtures were physically stable during compaction, but the
35 excipient selection affected the long term stability of the ibuprofen-arginine mixture. CARS and
36 SFG/SHG proved feasible techniques in imaging the component distribution on the tablet surfaces,
37 but possibly due to the limited imaging area, recrystallization detected with x-ray diffraction was
38 not detected.

39 **KEYWORDS:** Co-amorphous, amino acid, tablet, deformation, dissolution, multimodal non-linear
40 imaging, CARS, SFG, SHG

41 **ABBREVIATIONS¹**

¹ ACN, acetonitrile; ARG, arginine; CA, co-amorphous; CARS, coherent anti-Stokes Raman scattering; ER%, elastic recovery (%); FTIR, Fourier-transform infrared spectroscopy; HPLC, high-performance liquid chromatography; IBU, ibuprofen; IND, indomethacin; IR, infrared; KL, Kuentz-Leuenberger; PM, physical mixture; PVP, polyvinylpyrrolidone K30; SD, spray drying; SEM, scanning electron microscopy; SFG, sum frequency generation; TFA, trifluoro acetic acid; XRD, X-ray diffraction

42 1. INTRODUCTION

43 The majority of drugs currently under development possess poor water solubility, which may lead
44 to limited oral bioavailability as well as challenges in drug formulation and *in vitro* and *in vivo*
45 testing during drug development [1,2]. Transformation of a crystalline drug to the amorphous form
46 is a promising option for overcoming these challenges, since it has been shown to effectively
47 increase the apparent solubility and dissolution rate of poorly soluble drugs [3-5]. However, the use
48 of amorphous drugs has been limited due to their poor physical stability (i.e. tendency to
49 recrystallize).

50 To stabilize the amorphous form, different glass solution subtypes, i.e. polymeric amorphous solid
51 dispersions, mesoporous silicon or silica-based glass solutions, and co-amorphous formulations
52 have been introduced [4-9]. Of these formulations, the solid dispersions are the most extensively
53 studied, but during the last decade the interest towards co-amorphous formulations (i.e. single-phase
54 amorphous mixtures of the drug and two or more pharmaceutically active or inactive low molecular
55 weight substances) has increased due to the potential for good physical stability, combination
56 therapy and the reduced size of the final dosage form [4,7-10]. Additionally, co-amorphous
57 formulations (especially co-amorphous salts) have been shown to increase dissolution rates, and in
58 some studies even stabilize supersaturation, when compared to the crystalline or, more importantly,
59 to the pure amorphous drugs [9-13].

60 Being a relatively novel formulation approach, the co-amorphous mixtures have mainly been
61 prepared by small scale methods, but in recent years also preparation methods that can be scaled up,
62 such as spray drying (SD) and hot-melt extrusion, have been successfully utilized [9,14-19].

63 However, even though the co-amorphous systems are generally developed to improve the oral
64 bioavailability, the development of oral dosage forms containing co-amorphous mixtures is still in
65 its infancy [10,20]. Recently, some authors have successfully included co-amorphous mixtures in
66 tablet formulations [21-23], but the deformation properties of the co-amorphous mixtures and the

67 effect of tablet composition on tablet properties has remained unexplored, even though the
68 compaction properties of the co-amorphous components may differ from their crystalline
69 counterparts and the excipients may significantly affect the deformation properties, mechanical
70 strength, drug release as well as physical stability of the amorphous components [24-27].
71 Additionally, both Lenz et al. [21] and Petry et al. [22] investigated the physical stability of co-
72 amorphous indomethacin-arginine (IND-ARG) from ground tablets with conventional methods (X-
73 ray diffraction (XRD), Fourier-transform infrared spectroscopy (FTIR)), even though the
74 recrystallization may be more pronounced on the tablet surface, and it may be too otherwise limited
75 to be observed with conventional methods [27,28].

76 Non-linear optical imaging techniques, including coherent anti-Stokes Raman scattering (CARS)
77 and sum frequency/second harmonic generation (SFG/SHG) microscopies, are relatively new
78 imaging modalities with interesting capabilities. The general benefits of these techniques include
79 label-free, chemically-specific signal, fast data-acquisition time and inherent non-destructive
80 “confocal”- like imaging [29]. The label-free nature of CARS is based on the non-linear probing of
81 molecular vibrational resonances [30], whereas materials with non-centrosymmetric structures
82 generate SFG/SHG signals [31]. Most of the research in the use of non-linear optics has been
83 focused on instrument development, however studies of the applications of non-linear optical
84 imaging in different fields are increasing. Mostly, these techniques have been used in biomedical
85 applications, where especially CH₂ stretching of lipids has been probed with CARS [32], while
86 collagen has been imaged with SHG [33]. However, pharmaceutical applications including solid-
87 state analysis of non-linear optical imaging have also been increasing [29]. For example CARS has
88 been used to identify solid-state forms of IND on tablet surfaces [34,35] and to monitor the solid-
89 state changes of theophylline during dissolution [36]. On the other hand SFG/SHG, can be
90 especially useful in solid-state analysis, since only non-centrosymmetric crystals produce SFG/SHG
91 signals. SHG has been quantitatively used to analyse pharmaceutical solid-solid mixtures [37] and

92 has also been utilized in imaging, for example to visualize trace crystallinity in powder mixtures
93 with a detection limit of 4 ppm [38]. In multimodal non-linear optical imaging, CARS and
94 SFG/SHG can be simultaneously combined. It was recently shown that such a combination is well-
95 suited to the detection of different polymorphs and the amorphous form on tablet surfaces with high
96 sensitivity [35]. Crystallisation processes during storage can be imaged in detail. While in that study
97 tablets were composed of pure drug, the multimodal technique also has much potential for
98 analysing relatively complex multicomponent tablets. Multimodal CARS and SFG/SHG imaging
99 has not yet been used to image formulations containing both drug and excipient, nor changes in
100 their crystallinity and component distribution upon storage.

101 In the present study, we prepared tablets containing amorphous salts of ibuprofen (IBU) and ARG
102 and IND and ARG, and employed multi-modal non-linear optical imaging and established
103 analytical methods to explore the effect of formulation variables on pharmaceutical performance.
104 The tablet compositions were selected with an experimental design that consisted of three factors,
105 i.e. the amount of drug-ARG salt, the amount of polyvinylpyrrolidone K30 (PVP) and the sugar
106 alcohol species. Our aim was to investigate the effect of the abovementioned variables on the
107 compaction characteristics, on the mechanical properties of the tablets as well as on the drug release
108 behaviour and the physical stability of the co-amorphous salts. Additionally, CARS and SFG/SHG
109 were combined in order to explain compaction properties by visually detecting the drug and
110 excipient distribution and to detect possible phase separation and re-crystallization on the surface of
111 complex multi-component tablets during storage.

112 **2. MATERIALS AND METHODS**

113 **2.1 Materials**

114 ARG (L-enantiomer) and PVP were purchased from Sigma-Aldrich Co. (St. Louis, USA) and γ -
115 IND from Hangzhou Dayanchem (Hangzhou, China). Racemic R,S-IBU and the sugar alcohols

116 (mannitol (Pearlitol® 200SD) and xylitol (Xylisorb® 200DC)) were kindly donated by Orion
117 Corporation (Espoo, Finland) and Roquette (Lestrem, France), respectively. Glacial acetic acid
118 (Riedel de Haën, Seelze, Germany), hydrochloric acid (HCl, 37 %; Riedel-de-Haën, Seelze,
119 Germany), potassium chloride (J. T. Baker, Deventer, Holland), sodium acetate (Riedel-de-Haën,
120 Seelze, Germany), sodium hydroxide (NaOH; VWR Chemicals, Leuven, Belgium), and potassium
121 dihydrogen phosphate (KH₂PO₄; Merck, Darmstadt, Germany) were used in the preparation of the
122 buffer solutions. During the storage of the samples, dry conditions were maintained with
123 phosphorus pentoxide (P₂O₅), while approximately 33% RH was maintained with saturated
124 magnesium chloride (MgCl₂) solution. Ultrapurified water (class I; Elga Purelab Ultra, Elga
125 LabWater, UK) was used in the high-performance liquid chromatography (HPLC) mobile phase as
126 well as to prepare the drug-ARG solutions prior to the SD. Otherwise class II water (Elix 5,
127 Millipore S.A.S., Molsheim, France) was used throughout the study. Acetonitrile (ACN; HPLC
128 grade; VWR Chemicals, Leuven, Belgium and Fisher Chemical, Loughborough, UK) and trifluoro
129 acetic acid (TFA; HPLC-grade; Sigma-Aldrich, Germany) were the other components of the high
130 performance liquid chromatography (HPLC) mobile phase.

131 **2.2 Methods**

132 **2.2.1 Preparation of the co-amorphous salts**

133 The co-amorphous IBU-ARG and IND-ARG salts were prepared by spray drying as described in
134 our previous article [19]. Briefly, an amount of drug was dissolved in a corresponding amount of
135 5% ARG-water solution in order to obtain a drug-ARG molar ratio of 1:1, and once the solution
136 was visually clear, it was spray dried with a Büchi Mini Spray Dryer B-191 (Büchi Labortechnik
137 AG, Flawil, Switzerland). The water content of the freshly prepared samples was measured in
138 triplicate with a coulometric Karl-Fischer titrator (Mettler Toledo C30, Mettler-Toledo GmbH,
139 Greifensee, Switzerland). After preparation, the co-amorphous systems were stored in brown glass
140 jars under 4 °C 0% RH conditions until the tablets were prepared.

141 **2.2.2 Tablet composition and experiment design**

142 The tablet mixture compositions (Table 1) were based on a 2-level full factorial experiment design
143 with three centre points that was conducted with Modde Pro-software (11.0.1, MKS Umetrics AB,
144 Sweden). The experimental factors were drug load, amount of PVP, and the sugar alcohol species,
145 whereas the responses were tablet tensile strength, elastic recovery, $1/C$ -value from the Kuentz-
146 Leuenberger (KL) equation (Eq. 3, see section 2.2.5), the cumulative dissolved amount of drug after
147 15 min ($CDA_{15\text{min}}$), and the area under the cumulative dissolved drug amount-time curve after the
148 2h dissolution study ($AUC_{0-120\text{min}}$). The compaction force and the relative amount of the sugar
149 alcohol were kept constant (20 kN and 60% (m/m) of the tablet mass, respectively). Thus, the tablet
150 mass was changed according to the drug dose and the amount of PVP.

151 **2.2.3 Preparation of the powder mixtures**

152 The powder blends for tableting were prepared in a mortar by first mixing the drug-ARG mixture
153 with PVP and then adding the sugar alcohol in two or three batches depending on the amount of the
154 final mixture. The homogeneities of the prepared powder mixtures were investigated with two
155 model formulations (B4 and N2) by dissolving five parallel tablets in 250 ml of phosphate buffer
156 (pH 7.4) in ambient conditions and analysing the drug content with HPLC after 24h.

157 **2.2.4 Tablet preparation**

158 Flat faced tablets (diameter 13 mm) were compressed with a compaction simulator (PCS-1,
159 PuuMan Ltd., Kuopio, Finland) using a double-sided sine wave compression profile (duration 1500
160 ms). Due to high ejection forces, powder sticking and tablet fracturing occurred during preliminary
161 studies without lubrication, and thus magnesium stearate was added to the die walls and lower
162 punch using a brush prior to every compression except for the tablets for stability studies. The
163 compaction force was set to approximately 20 kN with every formulation. The tablets were weighed
164 immediately after compression, whereas the dimensions were measured the next day.

165 2.2.5 Compaction characteristics

166 The force-displacement data of five parallel compressions were collected and corrected according to
 167 the punch deformations. This corrected data was utilized to determine the relative density (ρ) of the
 168 different formulations at various compaction pressures according to Eq. 1:

$$\rho = \frac{\rho_{app}}{\rho_{t,mix}} \quad (1)$$

169 where ρ_{app} is the density at a certain pressure and $\rho_{t,mix}$ is the true density of the formulation that
 170 was calculated according to Eq. 2:

$$\rho_{t,mix} = \frac{w_1 + \dots + w_n}{\frac{w_1}{\rho_{t1}} + \dots + \frac{w_n}{\rho_{tn}}} \quad (2)$$

171 Here, w denotes weight fraction and ρ_t the true density, while the subscripts 1 and n refer to the
 172 different components of the formulation [40]. The ρ_t -values of the single components were obtained
 173 from the literature [41-43].

174 The deformation properties of the different formulations were evaluated using the KL-equation (Eq.
 175 3):

$$\sigma = \frac{1}{C} \left[\rho_c - \rho - (1 - \rho_c) \ln \left(\frac{1 - \rho}{1 - \rho_c} \right) \right] \quad (3)$$

176 where σ is the compaction pressure, $1/C$ is a plasticity parameter (interpretation corresponds to the
 177 yield pressure from Heckel equation) and ρ_c is the critical relative density (relative density where
 178 mechanical rigidity emerges in the powder bed) [44,45]. To determine the ρ_c , the pressure
 179 susceptibility (χ_p ; susceptibility of the powder bed to external pressure) at each data point was
 180 calculated using Eq. 4 after which the χ_p was plotted against relative density as described by Kuentz
 181 and Leuenberger [44]. The ρ_c was considered as the pressure where the χ_p began to systematically
 182 decrease with increasing ρ (an example shown in the supplementary material (Figures S1A and
 183 S1B)). Finally, the constant C was obtained by fitting Eq. 3 to the σ vs. ρ data (Figure S1C) using

184 nonlinear regression that was conducted with SigmaPlot 14.0 (Systat Software Inc., San Jose, CA,
185 USA).

$$\frac{d\rho}{d\sigma} = \chi_p(1 - \rho) \quad (4)$$

186

187 The percentage of axial elastic recovery ($ER\%$) was obtained by using Eq. 5 [46]:

$$ER\% = \frac{H - H_c}{H_c} \times 100\% \quad (5)$$

188 where H is the tablet height measured 24h after compression and H_c is the tablet height at maximum
189 pressure.

190 A universal tester (CT-5 tester, Engineering Systems, Nottingham, England) was used to determine
191 the crushing strengths of the tablets ($n = 5$) 24h after the compression. The tensile strengths (σ)
192 were calculated according to Eq. 6:

$$\sigma = \frac{2P}{\pi Dt} \quad (6)$$

193 where P is the applied load (crushing strength), D is the tablet diameter, and t is the tablet thickness
194 [47].

195 **2.2.6 Dissolution studies**

196 The dissolution studies were performed with Sotax AT6 and Sotax AT7 smart dissolution testers
197 (Sotax AG, Basel, Switzerland) equipped with paddle stirrers. Each tablet formulation was studied
198 in triplicate in 500 ml of dissolution medium (pH 1.2 HCl buffer for IBU-tablets and pH 5.0 acetate
199 buffer for IND tablets) that was kept at 37 °C and stirred at 50 rpm. The duration of the study was 2
200 hours, the samples were taken at 5 min, 10 min, 15 min, 30 min, 60 min, 90 min, and 120 min time
201 points, and the sample volume (5 ml) was replaced with buffer solution. The samples were filtered
202 through 0.22 μm membrane filters (Syringe filter 30 mm Dia, PES 0.22 μm Membrane, Sterile,

203 Porvair Sciences, Leatherhead, UK), and the drug concentration was analysed with HPLC (see
204 section 2.2.7). Prior to the HPLC analysis, the samples were diluted with ACN to reach ACN/H₂O-
205 ratio of 70/30, and if necessary, further dilution was conducted with 70/30 ACN/H₂O mixture to
206 obtain drug concentrations below 100 µg/ml.

207 The effect of the formation of amorphous state and the effect of ARG on the dissolution behaviour
208 of the drugs were investigated by performing the 2h dissolution studies with tablets corresponding
209 to B4 and N2 formulations but containing either physical mixtures of the crystalline drug and ARG
210 or only the crystalline drug (ARG replaced by mannitol) instead of the co-amorphous salt.
211 Additionally, to investigate the effect of PVP on the supersaturation stability of the co-amorphous
212 salts, a 24h dissolution study was conducted with B4- and N2-formulations as well as with
213 formulations corresponding to B4 and N2, but in which the PVP was replaced with excess mannitol.
214 In these studies, the samples were taken at 5 min, 10 min, 15 min, 30 min, 1 h, 2 h, 4 h, 6 h, 8 h and
215 24 h time points.

216 **2.2.7 HPLC**

217 The HPLC equipment consisted of Gilson 321 pump and Gilson UV-vis 151 detector (Gilson Inc.,
218 Middleton, WI, USA), Gilson 234 auto injector (Gilson, Roissy-en-France, France), and a reversed
219 phase column (Phenomenex Gemini NX 5u C18 110A, 250x4, 60 mm, sr. nr. 590531-19, USA)
220 with a pre-column. The mobile phase (70/30 ACN/H₂O acidified with 0.1% TFA) flow rate was 1.2
221 ml/min and the detection wavelengths were 221 nm for IBU and 225 nm for IND. The standard
222 solutions (1, 5, 25, 50, 75, and 100 µg/ml) were prepared in 70/30 ACN/H₂O-mixture and measured
223 with HPLC to obtain standard lines that were linear ($R^2 > 0.997$) in the examined concentration
224 range.

225 **2.2.8 Tablet characterization**

226 The tablet formulations were stored under 25 °C/33% RH to investigate the effect of compaction
227 and tablet composition on the physical stability of co-amorphous salts. XRD and FTIR were used as
228 standard methods to detect re-crystallization during the 20-week test period.

229 X-ray diffractograms were collected from intact tablet surfaces using a Bruker D8 Discover
230 diffractometer (Bruker AXS GmbH, Karlsruhe, Germany) with Cu K α radiation ($\lambda = 1.54 \text{ \AA}$) and a
231 motorized slit. An acceleration voltage of 40 kV and current of 40 mA were used to perform a scan
232 between 5 and 35° 2 θ with a scan speed of 0.1 s/step and step size of 0.011°. DIFFRAC.V3-
233 software (Bruker AXS GmbH) was utilized for data collection.

234 The attenuated total reflectance (ATR) FTIR measurements were conducted with Thermo Nicolet
235 Nexus 8700 spectrometer (Thermo Electron Corp., Madison, WI, USA) and with Nicolet iS50 FT-
236 IR spectrometer (Thermo Scientific, Madison, WI, USA). The spectra were collected over a
237 wavenumber range of 650-4000 cm⁻¹ as an average of 64 scans with the resolution of 4 cm⁻¹.
238 OMNIC-software (Thermo Scientific) was used for data collection and analysis.

239 Additionally, CARS and SFG/SHG microscopies were utilized as more novel non-linear imaging
240 methods to characterize the raw materials and to detect phase separation and recrystallization on the
241 tablet surface as well as to image the drug-excipient distribution on the tablet surface. A Leica TCS
242 SP8 CARS microscope (Leica Microsystems, Wetzlar, Germany) was used. Briefly, the imaging
243 system consisted of an inverted microscope with a laser-scanning confocal scan-head and
244 photomultiplier tube (PMT) and GaAsP hybrid (HyD) photodetectors. The Stokes beam (ω_S) for
245 CARS excitation was emitted from a Nd:YVO₄ solid-state laser (1064.5 nm) (picoEMERALD[®],
246 APE, Berlin, Germany). Laser source was integrated with an optical parametric oscillator (OPO)
247 that generated tunable pump/probe beams (ω_p and ω_{pr}). The bandwidth of the Stokes beam (ω_S) was
248 about 2-3 cm⁻¹ and the repetition rate was 80 MHz. The pulse duration was 7 ps for the Stokes and
249 5-6 ps for the pump (ω_p) and probe beams (ω_{pr}). The pump beam wavelength can be tuned so that
250 the energy difference between these beams corresponds to some molecular vibrational resonance.

251 The vibration is then probed with a probe photon, which can originate from the same beam as the
252 pump photon. These beams are coherently driven into the sample and wave mixing results in
253 generation of the fourth, blue-shifted, anti-Stokes photon (ω_{as}), which is then detected. A water-
254 immersion objective (25×0.95 NA) HCX IRAPO L (Leica) was used to focus the light onto the
255 sample that was placed on a microscope slide No. 1.5. Epi-CARS detection was used to collect anti-
256 Stokes signal using a nondescanned PMT detector, while another nondescanned PMT detector was
257 simultaneously used to collect epi-directed SFG/SHG signals with the bandpass filter $465\text{ nm} \pm 85$
258 nm. HeNe laser (633 nm) was also used to visualize the tablet surfaces as reflected light was
259 detected with a PMT detector. Images of 512×512 or 1024×1024 pixels were acquired with a
260 pixel dwell time of $1.2\ \mu\text{s}$ (scanning speed 400 Hz, line average 2). For the spectroscopic analysis,
261 the wavelength of the pump beam was systematically changed 33 times from 893 nm to 925 nm
262 covering the CARS shifts between 1804 cm^{-1} and 1417 cm^{-1} . The acquisition time for each spectral
263 scan was approximately 15 mins. CARS spectra in the figures are offset for clarity. Contrast was
264 adjusted individually for each image. The Leica Application Suite Advanced Fluorescence
265 (LASAF) was used for image acquisition and processing together with Fiji ImageJ (open-source
266 distribution), GNU Image Manipulation Program v2 (open-source distribution) and Origin 2018
267 (OriginLab, Northampton, Massachusetts, USA). RGB color images based on PCA were generated
268 as described elsewhere using MATLAB R2016a (MathWork, MA, USA) [35]. Briefly, spectral data
269 was mean centered and SNV corrected and the PC score values were normalized so that the
270 minimum PC score value was set to 0 and the maximum score value to 1 and all values in between
271 scaled linearly. PC1, PC2, and PC3 scores are represented by red, green, and blue coloring,
272 respectively.

273 To verify the morphological aspects observed with CARS, the fresh and stored (6 months) tablets as
274 well as the spray dried drug-ARG powders were imaged with scanning electron microscopy (SEM).
275 The morphology of the spray dried particles was micrographed with a field emission scanning

276 electron microscope (Zeiss Sigma HD VP, Carl Zeiss NTS, Cambridge, UK) using Everhart-
277 Thornley type secondary electron detector and a 30 μm aperture in high vacuum with acceleration
278 voltage of 4 kV. With the tablets, the images were obtained under low vacuum conditions (15 Pa
279 chamber pressure with dry nitrogen gas) with a VPSE G3 detector (Carl Zeiss NTS, Cambridge,
280 UK) and an acceleration voltage of 10 kV. The low vacuum (higher gas pressure) conditions were
281 used with the tablets, because the tablet height (2-3 mm) and the porous structure of the tablets
282 including microfractures decreased the electric conductivity of the specimen. The charge due to the
283 electron beam was eliminated with the nitrogen gas medium.

284 **2.2.9 Statistical analysis**

285 The effect of the selected tablet composition variables (factors) on the tablet properties (responses)
286 were investigated with multiple linear regression (MLR) using MODDE Pro-software (11.0.1, MKS
287 Umetrics AB, Sweden). A separate model was created for each response, and the non-significant
288 interaction terms were excluded to provide the best possible model. The goodness of fit (R^2) and
289 goodness of prediction (Q^2) were utilized to evaluate the models. In a good model, R^2 should gain
290 values close to 1, whereas a Q^2 above 0.5 indicates good predicting power [48,49].

291 GraphPad Prism 5.03 (GraphPad Software Inc., La Jolla, USA) was used for the determination of
292 the $\text{AUC}_{0-120\text{minS}}$ and to conduct single-factor ANOVA with Tukey's post-hoc test. The results of
293 the statistical analyses were considered significant if $p < 0.05$.

294 **3. Results and discussion**

295 **3.1 Tablet preparation**

296 *3.1.1 Spray drying*

297 The spray drying of IBU-ARG solution resulted in white and loosely packed powder, whereas the
298 spray dried IND-ARG powder was yellow and slightly denser packed. Both of the powders were

299 rather cohesive and non-free flowing and, according to the SEM images (Figure 1), the spray dried
300 particles were spherical in shape and possessed diameters from less than 1 μm to a few dozens of
301 micrometres, which is typical for spray dried materials [50]. The average yields of the spray drying
302 were 31% with IND-ARG and 42% with IBU-ARG, which were similar with the values of our
303 recent study (29.2%-34.4% [19]) but lower than the yield reported by Jensen et al. (~70% [16]).
304 Additionally, the moisture contents of the freshly prepared powders ($2.8\pm 0.6\%$ (IBU-ARG) and
305 $3.3\pm 0.2\%$ (IND-ARG)) were close to those reported previously for spray-dried IND-amino acid
306 mixtures (3-4% [16]), and this amount of water is probably due to the water reuptake from the
307 environment rather than incomplete drying, since similar values were also measured from ball-
308 milled samples [16].

309 *3.1.2 Preparation of the powder mixtures and tablet compaction*

310 The prepared drug-ARG-PVP-sugar alcohol mixtures were homogenous, at least in terms of drug
311 content (tested with B4- and N2-formulations), since relative standard deviations of the released
312 drug amounts between the parallel tablets were 5.7% with B4 and 4.0% with N2. However, neither
313 of the formulations released the full drug dose (84% and 91% released from B4 and N2,
314 respectively). The discrepancy between the theoretical drug content and actual released drug
315 amount from B4 and N2 formulations may indicate that the poor flow properties of the spray dried
316 mixtures resulted in challenges in the mixing process, i.e. sticking of the drug-ARG mixtures onto
317 the weighing boats, mixing cards and onto the rough mortar surfaces, rather than uneven drug-ARG
318 distribution in the powder mixture. Lenz et al. [21] avoided this challenge with spray dried IND-
319 ARG by combining it in a premixture with colloidal silicon dioxide that improved the powder flow
320 properties and probably decreased the surface adherence of IND-ARG. However, the additional
321 formulation components might have overcomplicated the analyses performed in the present study,
322 and thus, no premixture was prepared.

323 **3.2 Tablet properties**

324 3.2.1 Mechanical properties

325 The exact values for variables describing the mechanical properties of the different formulations are
326 presented in the supplementary material (Table S1). The tablets containing IND-ARG (N-
327 formulations) were slightly stronger than those containing IBU-ARG (B-formulations), but between
328 corresponding formulations the difference was statistically significant only with pairs B3-N1 and
329 B8-N4. With elastic recovery, no clear trend could be seen between the B and N formulations. The
330 plasticity parameter ($1/C$) was significantly higher with every N formulation when compared to the
331 corresponding (i.e. B1-N5, B2-N6, B3-N1, B4-N2, B5-N7, B6-N8, B7-N3, B8-N4) B formulations.
332 Also, the ρ_c values were slightly higher with IND-ARG formulations, but since the same value was
333 used for every parallel tablet, no statistical analysis could be made.

334 The tensile strengths (1.9-3.5 MPa; Table S1) of the tablets produced in the present study with a
335 compaction force of 20 kN (compaction pressure \sim 150 MPa) were in agreement with observations
336 of Lenz et al. [21], who reported tensile strengths of 2.0 and 4.5 MPa for tablets consisting of spray
337 dried IND-ARG, mannitol, croscarmellose sodium, colloidal silicon dioxide and magnesium
338 stearate that were compressed under pressures of 82.3 and 198.6, MPa respectively. The modelling
339 of the effect of the tablet composition on tensile strength was challenging especially with B-
340 formulations as indicated by summary of fit plots in the supplementary material (Figure S2), which
341 can probably be explained by the low variation in tensile strength values together with the relatively
342 large deviation between the parallel measurements. However, as observed also in previous research,
343 mannitol formed stronger tablets than xylitol (Figure 2) [51]. Other main factors were insignificant.
344 Additionally, despite the one significant interaction factor for the N-formulations (Figures 2 and 3
345 (1.)), the direction of the changes in tensile strength, caused by varied tablet composition, were well
346 estimated by the significant main factor.

347 According to Tanner et al. [52], elastic recovery values between inelastic (e.g. glucose or calcium
348 hydrogen phosphate) and highly elastic (e.g. starch) materials can vary from 1 to 18%. Thus, the

349 axial elastic recovery percentages obtained in the present study indicate that both B and N
350 formulations possessed low or moderate elasticity. Additionally, even though elastic recovery as
351 well as other compaction characteristics may depend not only on the material properties but also on
352 the processing factors such as compaction force or speed, the elastic behaviour of the B and N
353 formulations were in accordance with those reported for the single components [53-59].

354 The model characteristics R^2 and Q^2 (Figure S2) indicated that the modelling of the effect of tablet
355 composition on the elastic recovery could be more successful than the modelling of tensile strength.
356 The model prediction of decreasing elasticity with increasing amount of drug-ARG mixture (Figure
357 2) could be explained by the more efficient coverage of the excipient particles by the drug-ARG
358 mixture, which could enhance particle bonding either by increased plasticity or adsorbance of water
359 as observed with spray dried lactose [24,60]. However, due to the inconsistencies between the
360 models of B and N formulations (opposite effect of sugar alcohol species on the ER% (Figure 2), no
361 significant interactions in model for B formulations (Figure 2) vs. highly significant interactions
362 with N formulations (Figures 2 and S3)), the conclusions concerning the effect of tablet
363 composition on the elastic recovery must be made with caution.

364 In this study, the KL-equation was utilized instead of the widely used Heckel equation to evaluate
365 the deformation properties due to its suggested better reliability [45]. According to R^2 and Q^2 values
366 (Figure S2), the $1/C$ value could be modelled reliably for both B and N formulations. Additionally,
367 the interaction plots (Figure 3 (2. and 3.)) indicated that the direction of the change in the $1/C$ value
368 could be predicted reasonably well with the main factors. The sugar alcohol species had the most
369 prominent effect on the $1/C$ value (Figure 2), which could again be expected due to their high
370 proportion in the tablets. Xylitol resulted in lower $1/C$ values than mannitol, indicating higher
371 plasticity [45]. This seems contradictory with previously reported deformation properties of primary
372 mannitol and xylitol particles, but may be explained by sodium carboxymethyl cellulose (~2%)
373 included in Xylisorb® 200DC, which lowered the yield pressure of metformin hydrochloride, when

374 co-spray dried with the drug [51,61]. In addition to the sugar alcohol species, both amount of drug-
375 ARG mixture and amount of PVP affected the plasticity of the powder mixtures (Figure 2). The
376 linear regression analyses between $1/C$ values of formulations containing low and high percentages
377 (instead of absolute amounts) of drug-ARG mixture or PVP further indicated increased plasticity
378 with an increasing proportion of drug-ARG mixture (slopes: -6.9 (B2-B5), -0.04 (B4-B7), -8.0 (N2-
379 N3) and -3.2 (N6-N7)) and a decrease in plasticity with an increase in the proportion of PVP
380 (slopes: 6.9 (B2-B5), 0.04 (B4-B7), 7.9 (N2-N3) and 3.1 (N6-N7)). The effect of drug-ARG amount
381 on plasticity was consistent with previous studies in which plasticity increased with amorphous
382 components [24,62-64], but the increase in the plasticity with the decrease in the amount of PVP
383 was inconsistent with its previously reported plastic nature [65]. However, in the present study, the
384 increase PVP proportion accompanied a decrease in the amount of the apparently plastic drug-ARG
385 mixture, which may explain the inconsistency.

386 *3.2.2 Dissolution properties*

387 The cumulative amount of dissolved drug increased up to 30 min, after which it remained steady or
388 began to decrease (Figure 4). None of the B-formulations released the full drug dose, whereas with
389 the N-formulations six out of nine tablets exhibited over 90% drug release.

390 The $CDA_{15\text{min}}$ and $AUC_{0-120\text{min}}$ values of the different formulations are presented in the
391 supplementary material (Table S2). Since the B formulations were unable to release the full drug
392 dose, there was only limited deviation between the $AUC_{0-120\text{min}}$ values of the B-formulations.
393 However, the deviation was more pronounced in the $CDA_{15\text{min}}$ value between B formulations as
394 well as in both $AUC_{0-120\text{min}}$ and $CDA_{15\text{min}}$ values between the N formulations. Thus, only a rather
395 poor model (Q^2 -value 0.23) could be formed to predict the effect of different factors on the AUC_{0-}
396 120 of the B-formulations (not further analysed) but modelling of the $CDA_{15\text{min}}$ of B formulations as
397 well as $AUC_{0-120\text{min}}$ and $CDA_{15\text{min}}$ of N formulations was more successful (Q^2 -values of 0.58, 0.75

398 and 0.82, respectively (Figure S4)). As with the models predicting the mechanical properties, most
399 of the interaction plots (Figure 5) of the AUC_{0-120} and CDA_{15min} models revealed that the direction
400 of the change in the response could be predicted by the main coefficients, but the magnitude of the
401 change may be dependent on another interacting factor.

402 According to the model, the amount of drug-ARG mixture and PVP were the most prominent
403 factors affecting the $AUC_{0-120min}$ and CDA_{15min} of the N-formulations (Figure 6). The increase in
404 $AUC_{0-120min}$ by increasing the IND-ARG amount was expected, since this factor described the drug
405 load instead of relative drug amount. Surprisingly, the model showed a negative effect of increasing
406 amount of PVP on both $AUC_{0-120min}$ and CDA_{15min} , even though PVP has been reported to enhance
407 the dissolution properties and stabilize the supersaturation of IND both freely in solution and in
408 solid dispersions [66-68], and, also in the present study, the ability of PVP to stabilize the
409 supersaturation of IND was clearly demonstrated in the 24h dissolution test with N2 formulations
410 containing and lacking PVP (Figure 7D). Some authors have, however, reported decreased
411 dissolution with amorphous solid dispersions with high PVP-IND ratios when compared to a
412 formulations with low PVP-IND ratio [69,70]. This phenomenon was attributed to increased
413 viscosity, which may have also reduced the IND release in the present study. With the B
414 formulations, the amount of IBU-ARG had no significant effect on the CDA_{15min} , probably due to
415 the incomplete drug release. According to the model, an increase in the amount of PVP, however,
416 significantly increased the CDA_{15min} of the B formulations suggesting the positive effect of PVP on
417 IBU release, which has been reported previously [71].

418 The drug release from formulations containing co-amorphous mixtures was faster than from
419 formulations containing physical drug-ARG mixture or plain crystalline drug, even though ARG in
420 the physical mixtures also enhanced drug release (Figure 7A and B). Additionally, with the N2-
421 formulation, the presence of ARG and the formation of an amorphous system significantly
422 increased the cumulative dissolved amount of IND at the end of the dissolution study (7.7%, 57.0%

423 and 92.7% drug release from tablets containing plain IND, physical IND-ARG mixture and co-
424 amorphous IND-ARG salt, respectively). The drug release was highest also from the B2
425 formulation containing co-amorphous IBU-ARG (45.2%), but there was no significant difference in
426 the amount of released drug between tablets containing physical mixture or crystalline IBU (31.9%
427 and 25.5%, respectively). The enhanced IBU and IND dissolution upon formation of the co-
428 amorphous system has been attributed to both its amorphous nature as well as salt formation
429 between the acidic drug and basic ARG [11,16,19,72]. With IND-ARG, enhanced drug release also
430 from the tablet formulation has been observed previously [21]. However, in our previous study [19],
431 the IND-ARG physical mixture (crystalline components) and γ -IND seemed to result in similar
432 dissolution profiles, whereas in the present study, drug release was higher with the physical
433 mixture. This may be due to the *in situ* amorphization of IND-ARG, which has been previously
434 observed to occur in tablets containing an IND-ARG physical mixture [21,22]. Lenz et al. [21]
435 observed a colour change from white to yellow when tablets containing physical IND-ARG were
436 immersed in the dissolution medium as well as a clear supersaturation followed by a rapid decrease
437 in IND concentration (recrystallization). In the present study, the colour change could also be
438 observed, but the PVP added to the tablet formulation possibly inhibited drug precipitation from
439 supersaturated solution.

440 Based on the dissolution profiles from the 24h dissolution study (Figure 7C), the cumulative
441 dissolved amount of IBU from the B4-formulation containing PVP remained relatively constant
442 (~34 mg or 45%) between 15min and 24h, whereas with the tablets lacking PVP only ~11 mg
443 (15%) was released after 15 min of dissolution. However, the release of IBU from tablets without
444 PVP continued throughout the study, and at 24h, the difference in cumulative dissolved amounts
445 between tablets containing and lacking PVP was no longer significant. With the N2-formulation
446 (Figure 7D), the IND release from both tablets (with and without PVP) was relatively fast (~69 mg
447 (92%) after 15 min). However, with the formulation without PVP, the dissolved amount of IND

448 began to decrease already after 15 min, and from 2h onwards it was significantly lower than with
449 the formulation containing PVP. The cumulative dissolved IND from the N2-formulation
450 containing PVP decreased only slightly during the 24h. These observations clearly indicated the
451 solubilizing and precipitation inhibitory effects of PVP. With IND the precipitation inhibitory effect
452 of PVP has been attributed to crystal growth inhibition caused by adsorption of PVP on IND
453 surfaces, whereas with IBU the solubilization is due to the strong interactions between IBU and
454 PVP [67,73-82].

455 It has also been relatively unknown, if the co-amorphous formulations maintain their dissolution
456 advantage over for example PM or amorphous drug alone, when formulated as tablets [10].
457 However, based on the present study, even a relatively small addition of stabilizing polymer as a
458 physical mixture with co-amorphous powder might stabilize the supersaturation of the amorphous
459 drug. A similar observation was made by Petry et al. [22] by coating tablets containing co-
460 amorphous IND-ARG with a polymeric coating. However, even though the film coating was
461 applied to protect the formulation from moisture, the coating process itself causes various stresses
462 (heat, moisture, mechanical) to the formulation. Thus, incorporating the polymer to the tablet
463 formulation, as shown in the present work, might be suitable also for materials that cannot
464 withstand a coating process.

465 *3.2.3 Tablet characterization*

466 The stability studies were conducted with every formulation (B1-B9 and N1-N9), but since the
467 observations from the formulations containing the same drug-ARG mixture and sugar alcohol
468 resembled each other, the X-ray diffractograms and FTIR spectra of B2-, B4-, N2- and N6-

469 formulation are shown here as examples (Figure 8). The diffractograms and spectra of other
470 formulations can be found from the supplementary material (Figures S5 and S6).

471 At day 0, the majority of the diffractograms showed only peaks originating from either mannitol or
472 xylitol (Figure 8A and Figures S5 and S6), which indicates that despite the possible mechanical and
473 heat stresses [24,25], the co-amorphous salts were physically stable under compaction.

474 Additionally, no signs of recrystallization could be observed during the 20-week stability study in
475 the diffractograms of either the IBU-ARG formulations containing mannitol or any of the N
476 formulations. IND-ARG has been found to be highly stable under various conditions and as a pure
477 powder or when formulated as tablets [11,16,19,21,22]. Additionally, in our previous study [19],
478 co-amorphous IBU-ARG did not recrystallize over one year in dry conditions, but at 60% RH
479 liquefaction occurred. In the present study, the tablets retained their original appearance, and in the
480 tablets containing mannitol, the IBU-ARG mixture remained amorphous. However, already at day
481 0, the diffractogram of B1-formulation included a small peak appeared at approximately 16.8° (2θ),
482 which could be observed in the diffractograms of every formulation containing IBU-ARG and
483 xylitol after 6 weeks. Additionally, a peak at approximately 19.0° (2θ) emerged in almost every
484 diffractogram of these formulations. In the diffractograms from 12- and 20-week time points, these
485 peaks became more obvious, and a peak at approximately 6.0° (2θ) began to appear.

486 The IR spectra between $1400\text{-}1800\text{ cm}^{-1}$ of all the N-formulations and the spectra of mannitol
487 containing B-formulations corresponded to the spectra reported previously [16,19,21,72], and
488 remained unchanged during the 20 week stability study indicating salt formation between the
489 components as well as high physical stability (Figures 8B and S6). However, with B-formulations
490 containing xylitol, peak shifted and new peaks appeared (Figures 8B and S5). Instead of the broad
491 CN stretch band at 1540 cm^{-1} in the spectrum of co-amorphous IBU-ARG salt, a peak with two
492 maxima at 1566 and 1577 cm^{-1} appeared in the spectra of the stored B1-, B2-, B5-, B6- and B9-
493 formulations. These peaks may originate from the antisymmetric stretch of the ionized carboxylic

494 acid group of IBU as well as from the shifted CN-stretching vibration of ARG [72]. Additionally,
495 the peak at 1632 cm^{-1} (ARG guanidyl group stretching) and the shoulder at 1668 cm^{-1} (ARG COO⁻
496 and guanidyl group stretching) in the IBU-ARG spectrum had shifted to a peak at 1629 cm^{-1} and to
497 a shoulder at 1657 cm^{-1} , respectively, and a new shoulder appeared at 1704 cm^{-1} (IBU carbonyl
498 stretching). With B1-, B2-, B6- and B9-formulations, these changes occurred already after 6 weeks
499 of storage, and after 20 weeks they were present also in the spectrum of the B5-formulation
500 (samples were not measured at 12 weeks).

501 The peaks appearing in the diffractograms of the B formulations containing xylitol could be
502 attributed to either crystalline IBU (peaks at 6.1° , 16.6° , 16.7° and 19.0° (2θ)) or ARG (peaks at
503 16.8° and 19.1° (2θ)) (diffractograms not shown), but the components may also have crystallized as
504 a salt, as observed by Kasten et al. [83] with IND-lysine. Additionally, Petry et al. [84] observed the
505 formation of a crystalline IND-ARG salt after storing the IND-ARG physical mixture under 75%
506 RH. However, since we have been unable to produce crystalline IBU-ARG [19], no reference
507 diffractogram of crystalline IBU-ARG salt was available. The appearance of a shoulder at 1704 cm^{-1}
508 in the IR spectra of these formulations suggest that IBU had, at least partly, recrystallized as a free
509 acid. However, due to the other spectral changes, also the crystalline IBU-ARG salt may be present
510 in the xylitol containing IBU-ARG formulations. The presence of PVP complicates the analysis
511 further, since it interacts strongly with IBU and even solid-state *in situ* amorphization has been
512 observed [73,85,86]. Thus, the exact nature of the recrystallized species could not be resolved with
513 the current methods, and the coexistence of amorphous IBU-ARG together with crystalline IBU
514 and/or ARG and/or IBU-ARG salt seemed possible. However, xylitol reduced the physical stability
515 of co-amorphous IBU-ARG, possibly due to its higher hygroscopicity when compared to mannitol
516 [51].

517 Multimodal non-linear optical imaging, specifically involving CARS and SFG/SHG, was used to
518 visualize the tablet surfaces over the 20 week period. Crystalline arginine, xylitol and mannitol

519 exhibited strong SFG/SHG signals due to their non-centrosymmetric crystal structures. L-arginine
520 has a monoclinic crystal structure with space group $P2_1$ (CSD code TAQBIY [87]) and xylitol and
521 D-mannitol have orthorhombic crystal structures with space group $P2_12_12_1$ (CSD codes
522 XYLTOL04 [88] for xylitol and DMANTL08 [89] and DMANTL09 [90] for the alpha and beta
523 polymorphs of D-mannitol, respectively) [91-93]. The spray-dried co-amorphous mixtures and
524 centrosymmetric crystalline ibuprofen and gamma indomethacin did not exhibit SFG/SHG signals
525 (data not shown). Gamma indomethacin has a triclinic structure with space group $P\bar{1}$ (CSD code
526 INDMET03 [94]) and ibuprofen has a monoclinic structure with space group $P2_1/c$ (CSD code
527 IBPRAC06 [95]) [96,97]. The SFG/SHG activities of amorphous, gamma and alpha indomethacin,
528 their Raman and CARS spectra as well as the tendency of indomethacin to recrystallize to the
529 gamma-form under relatively dry conditions are known [35].

530 The CARS and Raman spectra of the co-amorphous IND-ARG mixture exhibited similarities to the
531 spectra of amorphous indomethacin with two distinguishable C=O stretching peaks at 1579 cm^{-1}
532 and 1676 cm^{-1} (Figure S7 A and B) [35,98]. Crystalline ibuprofen exhibited a distinguishable
533 CARS peak at 1603 cm^{-1} (Figure S7 B). This C-C stretching peak [99] typically moves to higher
534 Raman shifts when the ibuprofen is amorphous, for example in an amorphous solid dispersion with
535 PVP [100]. The CARS spectra of the co-amorphous mixture of IBU-ARG revealed this shift with
536 the peak at 1615 cm^{-1} (Figure S7 B and C). PVP exhibited its broad amide C=O stretching peak at
537 around $1640 - 1676\text{ cm}^{-1}$ (Figure S7 A and B) [101]. Xylitol and mannitol exhibited a CH_2
538 stretching peak at 1472 cm^{-1} and 1460 cm^{-1} in the CARS spectra, respectively [102] (Figure S7 A
539 and B). The CARS spectrum of arginine lacked any distinguishable peaks (Figure S7 A and B).

540 On the basis of these analyses, the distribution of different chemical components on tablet surfaces
541 could be imaged by combining CARS and SFG/SHG microscopies. Xylitol and mannitol could be
542 probed by SFG/SHG, while amorphous IND-ARG, IBU-ARG and PVP could be imaged using
543 CARS (Figure 9 and S9-13). In the images some regions appear darker than others due the surface

544 roughness of the tablets (the non-linear optical signal is generated only at the small focal point).
545 Since CARS spectra were measured on tablet surfaces, it was possible to use different approaches to
546 form images and extracted spectra from different regions could be further used to identify different
547 chemical and solid-state components spatially. A PCA based approach was successfully used to
548 visualize component distribution on the IBU-ARG tablet surfaces (formulations B2 and B4, Figure
549 9 A,D,G,I). However, the indomethacin signal from IND-ARG tablets was so dominant that a PCA
550 based approach was not able to identify PVP (data not shown). However, PVP could be
551 distinguished by visualizing the tablet surface using a single CARS shift at 1652 cm^{-1} (C=O
552 stretching specific to PVP) with supportive spectral information extracted from regions of interest
553 confirming the spectral profile of PVP (Figure S9). On the other hand spectral differences between
554 the PVP and drug-ARG mixtures could be utilized in fast narrowband single-shift CARS imaging,
555 together with simultaneous SFG/SHG imaging, as demonstrated in tile scan obtained from the IBU-
556 ARG formulation B2 (Figure S10).

557 The CARS and SEM images (Figure 9 and Figures S9-S12 and S14) suggest that the spray dried
558 particles were much more prominent on the surfaces of the freshly prepared tablets than could be
559 expected based on the high mass percentage of mannitol or xylitol. Additionally, the CARS images
560 indicated that the spray-dried particles were considerably smaller than the PVP and sugar alcohol
561 particles, and that the sugar alcohol particles as well as PVP particles were surrounded by the spray
562 dried particles. Barra et al. [103] reported the adherence of small excipient particles with preferable
563 compaction properties on larger poorly compacting drug particles, which resulted in enhanced
564 compaction properties of the mixture when compared to mixtures where no interactions existed
565 between the drug and excipient particles. Thus, the observations on component distribution based
566 on CARS images might have indicated a significant effect of the amount of drug-ARG mixtures on
567 the compaction properties of the powders as well as on the mechanical properties of the tablets.
568 However, the models predicting compaction and tablet properties suggested that the sugar alcohol

569 species was the most significant factor affecting the investigated responses and only with elastic
570 recovery, the model prediction could possibly be explained by the visual observations (i.e. coverage
571 of the sugar alcohol particles by the spray-dried particles). This discrepancy between model
572 predictions and visual observations may be explained by the small changes in the amounts of drug-
573 ARG mixtures when compared to the change of the entire sugar alcohol species. Thus, in the future,
574 it would be beneficial to perform compaction studies with larger variation in the amount of the
575 spray-dried material in order to verify the significance of the co-amorphous material on the
576 compaction process suggested by the CARS and SEM.

577 The most prominent difference between CARS/SFG/SHG images of IBU-ARG and IND-ARG
578 obtained over the 20 week period was the change in surface morphology, which was confirmed by
579 the SEM images from fresh and stored (6 months) tablets (Figures S11, S12 and S14). On day 0, the
580 co-amorphous drug-ARG particles could be clearly seen in both B- and N- formulations. However,
581 the surface of IBU-ARG tablets (B4- and B2- formulations) became smoother and individual
582 particles were not visible anymore. This change in surface morphology could be observed already
583 on week 4 (Figure S13) and smooth surface appearance remained over 20 week period (Figure 9).
584 However, CARS spectroscopy revealed that spectra extracted from tablet surfaces on day 0 and on
585 week 20 resembled closely each other in IBU-ARG formulations B4 and B2 (Figure 9) and IND-
586 ARG formulations N2 and N6 (Figure S9), thus any recrystallization in both IBU-ARG and IND-
587 ARG tablets was not observed with the non-linear optical imaging.

588 Since signs of recrystallization were observed in the B2 formulation with XRD and FTIR already
589 after 6 weeks of storage, these techniques were also used to measure the tablets imaged with CARS
590 after 14 and 20 weeks of storage (data not shown). After 14 weeks no crystallization was observed
591 with any of the formulations, but after 20 weeks a small peak at $16.9^\circ 2\theta$ appeared in the
592 diffractogram of B2 formulation and minor changes could also be observed in its IR spectrum. The
593 higher stability of the B2 formulation imaged with CARS when compared to the one examined with

594 XRD and FTIR may be due to the moisture absorption of the spray dried powder prior to the
595 compression, which was more pronounced during the preparation of the tablets for XRD and FTIR
596 than for the non-linear optical imaging. However, since recrystallization could also be detected with
597 XRD and FTIR in the B2 formulation imaged with CARS, it seems that the crystallisation was
598 limited and occurred outside the limited surface area (465x465 μm) probed with non-linear optical
599 imaging. Detection of recrystallization with CARS may also have been compromised by the lack of
600 reference IBU-ARG crystalline salt, although it is likely that the crystalline salt would have
601 exhibited some CARS spectral and/or SFG signal differences compared to the amorphous form.

602 One main benefit of coherent Raman imaging such as CARS with SFG/SHG microscopy is the
603 imaging speed. Tile scan shown in Figure S10 was composed of 20 1024×1024 pixel images
604 acquired at two CARS shifts 1652 cm^{-1} (PVP) and 1615 cm^{-1} (IBU-ARG) with a pixel dwell time of
605 $1.2 \mu\text{s}$ resulting in a total acquisition without laser tuning of approximately 1 min. Additionally,
606 data-acquisition time in spectral scan was approximately 15 min, whereas it can take up to hours to
607 perform spontaneous Raman mapping [104]. In the present study, it was shown that non-linear
608 optical imaging is well-suited to stability analysis of formulated tablet surfaces. Nevertheless,
609 confirming and thus imaging the chemical- and solid-state forms of different species requires non-
610 linear optical knowledge of the crystallizing species and proper reference materials.

611 **4. Conclusions**

612 In the present study, tablets of sufficient strength could be produced from both co-amorphous IBU-
613 ARG and IND-ARG salts, which also were found to be relatively physically stable during tablet
614 compaction, even though this may be affected by the excipients. However, based on the results of
615 the experimental design, mannitol could be recommended as a diluent for co-amorphous
616 formulations over xylitol, since mannitol produced stronger tablets with no recrystallization in any
617 of the formulations, whereas XRD and FTIR detected signs of recrystallization from tablets

618 containing IBU-ARG and xylitol. The drug release was more efficient from the tablets containing
619 co-amorphous mixtures when compared to physical mixtures, and a small amount of PVP added to
620 the formulation as a physical mixture was found to be effective in preventing drug recrystallisation
621 from supersaturated solutions, which might be useful with physically stable co-amorphous mixtures
622 that may be unable to stabilize supersaturation. In the present study, synergistic and simultaneous
623 CARS/SFG/SHG imaging/spectroscopy was successfully used to map different chemical
624 components on tablet surfaces. We were unable to detect phase separation or recrystallization of the
625 co-amorphous components due to their high physical stability. Thus, due to the capability of high
626 speed imaging of tablet surfaces, CARS and SFG/SHG are interesting options to complement the
627 traditional XRD and FTIR in physical stability monitoring.

628 **ACKNOWLEDGMENTS**

629 The authors thank Microscopy laboratory at SIB Labs, University of Eastern Finland for providing
630 laboratory facilities, PhD Jari Leskinen for SEM imaging and Master student Jarmo Maaranen for
631 his skilful technical assistance. RO acknowledges the support from the Doctoral Programme in
632 Drug Research in the Doctoral School of University of Eastern Finland as well as Nordforsk
633 (NordicPOP, project number 85352). JS and CS acknowledge the Academy of Finland (project
634 number 289398) and Business Finland (project number 462073).

635 **APPENDIX**

636 Supplementary data associated with this article can be found in the online version.

637

638

639 **REFERENCES**

- 640 [1] H.D. Williams, N.L. Trevaskis, S.A. Charman, R.M. Shanker, W.N. Charman, C.W. Pouton,
641 C.J. Porter, Strategies to address low drug solubility in discovery and development, *Pharmacol.*
642 *Rev.* 65 (2013) 315-499. doi: 10.1124/pr.112.005660.
- 643 [2] M. Rodriguez-Aller, D. Guillarme, J. Veuthey, R. Gurny, Strategies for formulating and
644 delivering poorly water-soluble drugs, *J. Drug Deliv. Sci. Technol.* 30 (2015) 342-351. doi:
645 10.1016/j.jddst.2015.05.009.
- 646 [3] B.C. Hancock, G. Zografi, Characteristics and Significance of the Amorphous State in
647 Pharmaceutical Systems, *J. Pharm. Sci.* 86 (1997) 1-12. doi: 10.1021/js9601896
- 648 [4] R. Laitinen, K. Löbmann, C.J. Strachan, H. Grohganz, T. Rades, Emerging trends in the
649 stabilization of amorphous drugs, *Int. J. Pharm.* 453 (2013) 65-79. doi:
650 10.1016/j.ijpharm.2012.04.066.
- 651 [5] P. Kanaujia, P. Poovizhi, W.K. Ng, R.B.H. Tan, Amorphous formulations for dissolution and
652 bioavailability enhancement of poorly soluble APIs, *Powder Technol.* 285 (2015) 2-15. doi:
653 10.1016/j.powtec.2015.05.012.
- 654 [6] K.K. Qian, R.H. Bogner, Application of mesoporous silicon dioxide and silicate in oral
655 amorphous drug delivery systems, *J. Pharm. Sci.* 101 (2012) 444-463. doi: 10.1002/jps.22779.
- 656 [7] H. Grohganz, P.A. Priemel, K. Löbmann, L.H. Nielsen, R. Laitinen, A. Mullertz, G. Van den
657 Mooter, T. Rades, Refining stability and dissolution rate of amorphous drug formulations, *Expert*
658 *Opin. Drug Deliv.* 11 (2014) 977-989. doi: 10.1517/17425247.2014.911728.
- 659 [8] S. Baghel, H. Cathcart, N.J. O'Reilly, Polymeric Amorphous Solid Dispersions: A Review of
660 Amorphization, Crystallization, Stabilization, Solid-State Characterization, and Aqueous
661 Solubilization of Biopharmaceutical Classification System Class II Drugs, *J. Pharm. Sci.* 105
662 (2016) 2527-2544. doi: 10.1016/j.xphs.2015.10.008.
- 663 [9] S.J. Dengale, H. Grohganz, T. Rades, K. Löbmann, Recent advances in co-amorphous drug
664 formulations, *Adv. Drug Deliv. Rev.* 100 (2016) 116-125. doi: 10.1016/j.addr.2015.12.009.
- 665 [10] R. Laitinen, K. Löbmann, H. Grohganz, P. Priemel, C.J. Strachan, T. Rades, Supersaturating
666 drug delivery systems: The potential of co-amorphous drug formulations, *Int. J. Pharm.* 532 (2017)
667 1-12. doi: 10.1016/j.ijpharm.2017.08.123.
- 668 [11] K. Löbmann, H. Grohganz, R. Laitinen, C. Strachan, T. Rades, Amino acids as co-amorphous
669 stabilizers for poorly water soluble drugs-Part 1: preparation, stability and dissolution enhancement,
670 *Eur. J. Pharm. Biopharm.* 85 (2013) 873-881. doi: 10.1016/j.ejpb.2013.03.014.
- 671 [12] R. Ojarinta, A.T. Heikkinen, E. Sievänen, R. Laitinen, Dissolution behavior of co-amorphous
672 amino acid-indomethacin mixtures: The ability of amino acids to stabilize the supersaturated state
673 of indomethacin, *Eur. J. Pharm. Biopharm.* 112 (2017) 85-95. doi: 10.1016/j.ejpb.2016.11.023.

- 674 [13] W. Wu, K. Löbmann, T. Rades, H. Grohgan, On the role of salt formation and structural
675 similarity of co-formers in co-amorphous drug delivery systems, *Int. J. Pharm.* 535 (2018) 86-94.
676 doi: 10.1016/j.ijpharm.2017.10.057.
- 677 [14] G. Craye, K. Löbmann, H. Grohgan, T. Rades, R. Laitinen, Characterization of Amorphous
678 and Co-Amorphous Simvastatin Formulations Prepared by Spray Drying, *Molecules* 20 (2015)
679 21532-21548. doi: 10.3390/molecules201219784.
- 680 [15] A. Beyer, L. Radi, H. Grohgan, K. Löbmann, T. Rades, C.S. Leopold, Preparation and
681 recrystallization behavior of spray-dried co-amorphous naproxen-indomethacin, *Eur. J. Pharm.*
682 *Biopharm.* 104 (2016) 72-81. doi: 10.1016/j.ejpb.2016.04.019.
- 683 [16] K.T. Jensen, L.I. Blaabjerg, E. Lenz, A. Bohr, H. Grohgan, P. Kleinebudde, T. Rades, K.
684 Löbmann, Preparation and characterization of spray-dried co-amorphous drug-amino acid salts, *J.*
685 *Pharm. Pharmacol.* 68 (2016) 615-624. doi: 10.1111/jphp.12458.
- 686 [17] L. Arnfast, M. Kamruzzaman, K. Löbmann, J. Aho, S. Baldursdottir, T. Rades, J. Rantanen,
687 Melt Extrusion of High-Dose Co-Amorphous Drug-Drug Combinations, *Pharm. Res.* (2017) 1-9.
688 doi: 10.1007/s11095-017-2254-8.
- 689 [18] E. Lenz, K. Löbmann, T. Rades, K. Knop, P. Kleinebudde, Hot Melt Extrusion and Spray
690 Drying of Co-amorphous Indomethacin-Arginine With Polymers, *J. Pharm. Sci.* 106 (2017) 302-
691 312. doi: 10.1016/j.xphs.2016.09.027.
- 692 [19] R. Ojarinta, L. Lerminiaux, R. Laitinen, Spray drying of poorly soluble drugs from aqueous
693 arginine solution, *Int. J. Pharm.* 532 (2017) 289-298. doi: 10.1016/j.ijpharm.2017.09.015.
- 694 [20] R.B. Chavan, R. Thipparaboina, D. Kumar, N.R. Shastri, Co amorphous systems: A product
695 development perspective, *Int. J. Pharm.* 515 (2016) 403-415. doi: 10.1016/j.ijpharm.2016.10.043.
- 696 [21] E. Lenz, K.T. Jensen, L.I. Blaabjerg, K. Knop, H. Grohgan, K. Löbmann, T. Rades, P.
697 Kleinebudde, Solid-state properties and dissolution behaviour of tablets containing co-amorphous
698 indomethacin-arginine, *Eur. J. Pharm. Biopharm.* 96 (2015) 44-52. doi: 10.1016/j.ejpb.2015.07.011.
- 699 [22] I. Petry, K. Löbmann, H. Grohgan, T. Rades, C.S. Leopold, Solid state properties and drug
700 release behavior of co-amorphous indomethacin-arginine tablets coated with Kollicoat® Protect,
701 *Eur. J. Pharm. Biopharm.* 119 (2017) 150-160. doi: 10.1016/j.ejpb.2017.06.007.
- 702 [23] Renuka, S.K. Singh, M. Gulati, R. Narang, Stable amorphous binary systems of glipizide and
703 atorvastatin powders with enhanced dissolution profiles: formulation and characterization, *Pharm.*
704 *Dev. Technol.* 22 (2017) 13-25. doi: 10.3109/10837450.2015.1125921.
- 705 [24] S. Patel, A.M. Kaushal, A.K. Bansal, Compression physics in the formulation development of
706 tablets, *Crit. Rev. Ther. Drug Carrier Syst.* 23 (2006) 1-65. doi:
707 10.1615/CritRevTherDrugCarrierSyst.v23.i1.10
- 708 [25] B. Demuth, Z.K. Nagy, A. Balogh, T. Vigh, G. Marosi, G. Verreck, I. Van Assche, M.E.
709 Brewster, Downstream processing of polymer-based amorphous solid dispersions to generate tablet
710 formulations, *Int. J. Pharm.* 486 (2015) 268-286. doi: 10.1016/j.ijpharm.2015.03.053.

- 711 [26] A. Agrawal, M. Dudhedia, W. Deng, K. Shepard, L. Zhong, E. Povilaitis, E. Zimny,
712 Development of Tablet Formulation of Amorphous Solid Dispersions Prepared by Hot Melt
713 Extrusion Using Quality by Design Approach, *AAPS PharmSciTech* 17 (2016) 214-232. doi:
714 10.1208/s12249-015-0472-0.
- 715 [27] P.T. Mah, D. Novakovic, J. Saarinen, S. Van Landeghem, L. Peltonen, T. Laaksonen, A.
716 Isomäki, C.J. Strachan, Elucidation of Compression-Induced Surface Crystallization in Amorphous
717 Tablets Using Sum Frequency Generation (SFG) Microscopy, *Pharm. Res.* 34 (2017) 957-970. doi:
718 10.1007/s11095-016-2046-6.
- 719 [28] N.K. Thakral, S. Mohapatra, G.A. Stephenson, R. Suryanarayanan, Compression-induced
720 crystallization of amorphous indomethacin in tablets: Characterization of spatial heterogeneity by
721 two-dimensional X-ray diffractometry, *Mol. Pharm.* 12 (2015) 253-263. doi: 10.1021/mp5005788.
- 722 [29] C.J. Strachan, M. Windbergs, H.L. Offerhaus, Pharmaceutical applications of non-linear
723 imaging, *Int. J. Pharm.* 417 (2011) 163-172. doi: 10.1016/j.ijpharm.2010.12.017.
- 724 [30] J.X. Cheng, X.S. Xie, Coherent anti-Stokes Raman scattering microscopy: Instrumentation,
725 theory, and applications, *J. Phys. Chem. B* 108 (2004) 827-840. doi: 10.1021/jp035693v
- 726 [31] P.J. Campagnola, A.C. Millard, M. Terasaki, P.E. Hoppe, C.J. Malone, W.A. Mohler, Three-
727 dimensional high-resolution second-harmonic generation imaging of endogenous structural proteins
728 in biological tissues, *Biophys. J.* 82 (2002) 493-508. doi: 10.1016/S0006-3495(02)75414-3.
- 729 [32] J.X. Cheng, X.S. Xie, Vibrational spectroscopic imaging of living systems: An emerging
730 platform for biology and medicine, *Science* 350 (2015) doi: 10.1126/science.aaa8870.
- 731 [33] J. Pirhonen, J. Arola, S. Sädevirta, P. Luukkonen, S. Karppinen, T. Pihlajaniemi, A. Isomäki,
732 M. Hukkanen, H. Yki-Järvinen, E. Ikonen, Continuous Grading of Early Fibrosis in NAFLD Using
733 Label-Free Imaging: A Proof-of-Concept Study, *PLoS One* 11 (2016) e0147804. doi:
734 10.1371/journal.pone.0147804.
- 735 [34] C.M. Hartshorn, Y.J. Lee, C.H. Camp, Z. Liu, J. Heddleston, N. Canfield, T.A. Rhodes, A.R.
736 Hight Walker, P.J. Marsac, M.T. Cicerone, Multicomponent chemical imaging of pharmaceutical
737 solid dosage forms with broadband CARS microscopy, *Anal. Chem.* 85 (2013) 8102-8111. doi:
738 10.1021/ac400671p.
- 739 [35] D. Novakovic, J. Saarinen, T. Rojalin, O. Antikainen, S.J. Fraser-Miller, T. Laaksonen, L.
740 Peltonen, A. Isomäki, C.J. Strachan, Multimodal Nonlinear Optical Imaging for Sensitive Detection
741 of Multiple Pharmaceutical Solid-State Forms and Surface Transformations, *Anal. Chem.* 89 (2017)
742 11460-11467. doi: 10.1021/acs.analchem.7b02639.
- 743 [36] A. Fussell, E. Garbacik, H. Offerhaus, P. Kleinebudde, C. Strachan, In situ dissolution analysis
744 using coherent anti-Stokes Raman scattering (CARS) and hyperspectral CARS microscopy, *Eur. J.*
745 *Pharm. Biopharm.* 85 (2013) 1141-1147. doi: 10.1016/j.ejpb.2013.08.012.
- 746 [37] C.J. Strachan, T. Rades, C.J. Lee, Determination of the optical second harmonic response of
747 pharmaceutical solid-solid mixtures, *Opt. Lasers Eng.* 43 (2005) 209-220. doi:
748 10.1016/j.optlaseng.2004.06.004.

- 749 [38] D. Wanapun, U.S. Kestur, L.S. Taylor, G.J. Simpson, Single Particle Nonlinear Optical
750 Imaging of Trace Crystallinity in an Organic Powder, *Anal. Chem.* 83 (2011) 4745-4751. doi:
751 10.1021/ac1031397.
- 752 [39] J.C. Parajó, H. Domínguez, J.M. Domínguez, Biotechnological production of xylitol. Part 1:
753 Interest of xylitol and fundamentals of its biosynthesis, *Bioresour. Technol.* 65 (1998) 191-201. doi:
754 10.1016/S0960-8524(98)00038-8.
- 755 [40] J. Hellrup, J. Nordström, D. Mahlin, Powder compression mechanics of spray-dried lactose
756 nanocomposites, *Int. J. Pharm.* 518 (2017) 1-10. doi: 10.1016/j.ijpharm.2016.12.041.
- 757 [41] R.C. Rowe, P.J. Sheskey, C. Owen Siân (Eds.), *Handbook of Pharmaceutical Excipients*, 5th
758 ed., Pharmaceutical Press and American Pharmacists Association, London, 2006.
- 759 [42] X. Cao, N. Leyva, S.R. Anderson, B.C. Hancock, Use of prediction methods to estimate true
760 density of active pharmaceutical ingredients, *Int. J. Pharm.* 355 (2008) 231-237. doi:
761 10.1016/j.ijpharm.2007.12.012.
- 762 [43] E. Berlin, M.J. Pallansch, Densities of several proteins and L-amino acids in the dry state. *J.*
763 *Phys. Chem.* 72 (1968) 1887-1889. doi: 10.1021/j100852a004
- 764 [44] M. Kuentz, H. Leuenberger, Pressure susceptibility of polymer tablets as a critical property: A
765 modified Heckel equation, *J. Pharm. Sci.* 88 (1999) 174-179. doi: 10.1021/js980369a.
- 766 [45] S. Paul, C.C. Sun, The suitability of common compressibility equations for characterizing
767 plasticity of diverse powders, *Int. J. Pharm.* 532 (2017) 124-130. doi:
768 10.1016/j.ijpharm.2017.08.096.
- 769 [46] N.A. Armstrong, R.F. Haines-Nutt, Elastic recovery and surface area changes in compacted
770 powder systems, *Powder Technol.* 9 (1974) 287-290. doi: 10.1016/0032-5910(74)80054-9.
- 771 [47] J.T. Fell, J.M. Newton, Determination of Tablet Strength by the Diametral-Compression Test,
772 *J. Pharm. Sci.* 59 (1970) 688-691. doi: 10.1002/jps.2600590523
- 773 [48] N. Willecke, A. Szepes, M. Wunderlich, J.P. Remon, C. Vervaet, T. De Beer, A novel
774 approach to support formulation design on twin screw wet granulation technology: Understanding
775 the impact of overarching excipient properties on drug product quality attributes, *Int. J. Pharm.* 545
776 (2018) 128-143. doi: 10.1016/j.ijpharm.2018.04.017.
- 777 [49] MODDE 11 User Guide, MKS Umetrics AB, Sweden
- 778 [50] R. Vehring, Pharmaceutical particle engineering via spray drying, *Pharm. Res.* 25 (2008) 999-
779 1022. doi: 10.1007/s11095-007-9475-1.
- 780 [51] G.K. Bolhuis, E.G. Rexwinkel, K. Zuurman, Polyols as filler-binders for disintegrating tablets
781 prepared by direct compaction, *Drug Dev. Ind. Pharm.* 35 (2009) 671-677. doi:
782 10.1080/03639040802587799.

- 783 [52] T. Tanner, O. Antikainen, H. Ehlers, D. Blanco, J. Yliruusi, Examining mechanical properties
784 of various pharmaceutical excipients with the gravitation-based high-velocity compaction analysis
785 method, *Int. J. Pharm.* 539 (2018) 131-138. doi: 10.1016/j.ijpharm.2018.01.048
- 786 [53] P.V. Marshall, P. York, J.Q. Maclaine, An investigation of the effect of the punch velocity on
787 the compaction properties of ibuprofen, *Powder Technol.* 74 (1993) 171-177. doi: 10.1016/0032-
788 5910(93)87009-D.
- 789 [54] L.E. Morris, J.C. Moore, J.B. Schwartz, Characterization and performance of a new direct
790 compression excipient for chewable tablets: Xylitab®, *Drug Dev. Ind. Pharm.* 22 (1996) 925-932.
791 doi: 10.3109/03639049609065922.
- 792 [55] P. Di Martino, M. Beccerica, E. Joiris, G.F. Palmieri, A. Gayot, S. Martelli, Influence of
793 crystal habit on the compression and densification mechanism of ibuprofen, *J. Cryst. Growth* 243
794 (2002) 345-355. doi: 10.1016/S0022-0248(02)01523-3.
- 795 [56] V. Mazel, V. Busignies, H. Diarra, P. Tchoreloff, On the links between elastic constants and
796 effective elastic behavior of pharmaceutical compacts: Importance of poisson's ratio and use of bulk
797 modulus, *J. Pharm. Sci.* 102 (2013) 4009-4014. doi: 10.1002/jps.23710.
- 798 [57] A. Nokhodchi, J.L. Ford, P.H. Rowe, M.H. Rubinstein, The effects of compression rate and
799 force on the compaction properties of different viscosity grades of hydroxypropylmethylcellulose
800 2208, *Int. J. Pharm.* 129 (1996) 21-31. doi: 10.1016/0378-5173(95)04236-9.
- 801 [58] O.F. Akande, M.H. Rubinstein, P.H. Rowe, J.L. Ford, Effect of compression speeds on the
802 compaction properties of a 1:1 paracetamol-microcrystalline cellulose mixture prepared by single
803 compression and by combinations of pre-compression and main-compression, *Int. J. Pharm.* 157
804 (1997) 127-136. doi: 10.1016/S0378-5173(97)00185-3.
- 805 [59] H. Larhrib, J.I. Wells, M.H. Rubinstein, Compressing polyethylene glycols: The effect of
806 compression pressure and speed, *Int. J. Pharm.* 147 (1997) 199-205. doi: 10.1016/S0378-
807 5173(96)04818-1.
- 808 [60] J. Ruangchayajatuporn, T. Amornsakchai, N. Sinchaipanid, A. Mitrevej, Compaction behavior
809 and optimization of spray-dried lactose with various amorphous content, *J. Drug Deliv. Sci.*
810 *Technol.* 21 (2011) 175-181. doi: 10.1016/S1773-2247(11)50019-X.
- 811 [61] N. Al-Zoubi, F. Odeh, I. Nikolakakis, Co-spray drying of metformin hydrochloride with
812 polymers to improve compaction behavior, *Powder Technol.* 307 (2017) 163-174. doi:
813 10.1016/j.powtec.2016.11.027
- 814 [62] T. Suzuki, H. Nakagami, Effect of crystallinity of microcrystalline cellulose on the
815 compactability and dissolution of tablets, *Eur. J. Pharm. Biopharm.* 47 (1999) 225-230. doi:
816 10.1016/S0939-6411(98)00102-7.
- 817 [63] A.R. Paradkar, B. Chauhan, S. Yamamura, A.P. Pawar, Preparation and characterization of
818 glassy celecoxib, *Drug Dev. Ind. Pharm.* 29 (2003) 739-744. doi: 10.1081/DDC-120021773.
- 819 [64] A.B. Joshi, S. Patel, A.M. Kaushal, A.K. Bansal, Compaction studies of alternate solid forms
820 of celecoxib, *Adv. Powder Technol.* 21 (2010) 452-460. doi: 10.1016/j.apt.2010.01.006.

- 821 [65] J. Rojas, S. Hernandez, Effect of the compaction platform on the densification parameters of
822 tableting excipients with different deformation mechanisms, *Chem. Pharm. Bull.* 62 (2014) 281-
823 287. doi: 10.1248/cpb.c13-00884.
- 824 [66] A. Forster, J. Hempenstall, T. Rades, Characterization of glass solutions of poorly water-
825 soluble drugs produced by melt extrusion with hydrophilic amorphous polymers, *J. Pharm.*
826 *Pharmacol.* 53 (2001) 303-315. doi: 10.1211/0022357011775532.
- 827 [67] S.A. Surwase, L. Itkonen, J. Aaltonen, D. Saville, T. Rades, L. Peltonen, C.J. Strachan,
828 Polymer incorporation method affects the physical stability of amorphous indomethacin in aqueous
829 suspension, *Eur. J. Pharm. Biopharm.* 96 (2015) 32-43. doi: 10.1016/j.ejpb.2015.06.005.
- 830 [68] R. Paus, A. Prudic, Y. Ji, Influence of excipients on solubility and dissolution of
831 pharmaceuticals, *Int. J. Pharm.* 485 (2015) 277-287. doi: 10.1016/j.ijpharm.2015.03.004.
- 832 [69] R.J. Chokshi, N.H. Shah, H.K. Sandhu, A.W. Malick, H. Zia, Stabilization of low glass
833 transition temperature indomethacin formulations: Impact of polymer-type and its concentration, *J.*
834 *Pharm. Sci.* 97 (2008) 2286-2298. doi: 10.1002/jps.21174.
- 835 [70] W. Zhang, C. Zhang, Y. He, B. Duan, G. Yang, W. Ma, Y. Zhang, Factors Affecting the
836 Dissolution of Indomethacin Solid Dispersions, *AAPS PharmSciTech* 18 (2017) 3258-3273. doi:
837 10.1208/s12249-017-0813-2.
- 838 [71] N.M. Najib, M. Suleiman, A. Malakh, Characteristics of the in vitro release of ibuprofen from
839 polyvinylpyrrolidone solid dispersions, *Int. J. Pharm.* 32 (1986) 229-236. doi: 10.1016/0378-
840 5173(86)90183-3.
- 841 [72] K. Löbmann, R. Laitinen, C. Strachan, T. Rades, H. Grohganz, Amino acids as co-amorphous
842 stabilizers for poorly water-soluble drugs-Part 2: molecular interactions, *Eur. J. Pharm. Biopharm.*
843 85 (2013) 882-888. doi: 10.1016/j.ejpb.2013.03.026.
- 844 [73] M.A. El-Hinnawi, N.M. Najib, Ibuprofen-polyvinylpyrrolidone dispersions. Proton nuclear
845 magnetic resonance and infrared studies, *Int. J. Pharm.* 37 (1987) 175-177. doi: 10.1016/0378-
846 5173(87)90024-X.
- 847 [74] N.M. Najib, M.A. El-Hinnawi, M.S. Suleiman, Physicochemical characterization of ibuprofen-
848 polyvinylpyrrolidone dispersions, *Int. J. Pharm.* 45 (1988) 139-144. doi: 10.1016/0378-
849 5173(88)90042-7.
- 850 [75] Z. Gashi, R. Censi, L. Malaj, R. Gobetto, M. Mozzicafreddo, M. Angeletti, A. Masic, P. Di
851 Martino, Differences in the interaction between aryl propionic acid derivatives and
852 poly(vinylpyrrolidone) K30: A multi-methodological approach, *J. Pharm. Sci.* 98 (2009) 4216-
853 4228. doi: 10.1002/jps.21734.
- 854 [76] L. Malaj, R. Censi, M. Mozzicafreddo, L. Pellegrino, M. Angeletti, R. Gobetto, P. Di Martino,
855 Influence of relative humidity on the interaction between different aryl propionic acid derivatives
856 and poly(vinylpyrrolidone) K30: Evaluation of the effect on drug bioavailability, *Int. J. Pharm.* 398
857 (2010) 61-72. doi: 10.1016/j.ijpharm.2010.07.024.

- 858 [77] K.P.R. Chowdary, D. Udaya Chandra, V. Parimala, M. Indira, A factorial study on formulation
859 development of ibuprofen tablets employing starch 1500 and PVP K 30, *Int. J. Pharm. Sci. Res.* 3
860 (2012) 189-193. doi: 10.13040/IJPSR.0975-8232.3(1).189-93
- 861 [78] H. Chauhan, A. Kuldipkumar, T. Barder, A. Medek, C.H. Gu, E. Atef, Correlation of
862 inhibitory effects of polymers on indomethacin precipitation in solution and amorphous solid
863 crystallization based on molecular interaction, *Pharm. Res.* 31 (2014) 500-515. doi:
864 10.1007/s11095-013-1178-1.
- 865 [79] D. Prasad, H. Chauhan, E. Atef, Amorphous stabilization and dissolution enhancement of
866 amorphous ternary solid dispersions: Combination of polymers showing drug-polymer interaction
867 for synergistic effects, *J. Pharm. Sci.* 103 (2014) 3511-3523. doi: 10.1002/jps.24137.
- 868 [80] D. Prasad, H. Chauhan, E. Atef, Role of Molecular Interactions for Synergistic Precipitation
869 Inhibition of Poorly Soluble Drug in Supersaturated Drug-Polymer-Polymer Ternary Solution, *Mol.*
870 *Pharm.* 13 (2016) 756-765. doi: 10.1021/acs.molpharmaceut.5b00655.
- 871 [81] D.D. Patel, B.D. Anderson, Adsorption of Polyvinylpyrrolidone and its Impact on Maintenance
872 of Aqueous Supersaturation of Indomethacin via Crystal Growth Inhibition, *J. Pharm. Sci.* 104
873 (2015) 2923-2933. doi: 10.1002/jps.24493.
- 874 [82] D. Hirai, Y. Iwao, S.I. Kimura, S. Noguchi, S. Itai, Mathematical model to analyze the
875 dissolution behavior of metastable crystals or amorphous drug accompanied with a solid-liquid
876 interface reaction, *Int. J. Pharm.* 522 (2017) 58-65. doi: 10.1016/j.ijpharm.2017.02.050.
- 877 [83] G. Kasten, K. Nouri, H. Grohganz, T. Rades, K. Löbmann, Performance comparison between
878 crystalline and co-amorphous salts of indomethacin-lysine, *Int. J. Pharm.* 533 (2017) 138-144. doi:
879 10.1016/j.ijpharm.2017.09.063
- 880 [84] I. Petry, K. Löbmann, H. Grohganz, T. Rades, C.S. Leopold, Undesired co-amorphisation of
881 indomethacin and arginine during combined storage at high humidity conditions, *Int. J. Pharm.* 544
882 (2018) 172-180. doi: 10.1016/j.ijpharm.2018.04.026.
- 883 [85] H. Sekizaki, K. Danjo, H. Eguchi, Y. Yonezawa, H. Sunada, A. Otsuka, Solid-State Interaction
884 of Ibuprofen with Polyvinylpyrrolidone, *Chem. Pharm. Bull.* 43 (1995) 988-993. doi:
885 10.1248/cpb.43.988.
- 886 [86] S. Bogdanova, I. Pajeva, P. Nikolova, I. Tsakovska, B. Müller, Interactions of
887 poly(vinylpyrrolidone) with ibuprofen and naproxen: Experimental and modeling studies, *Pharm.*
888 *Res.* 22 (2005) 806-815. doi: 10.1007/s11095-005-2598-3.
- 889 [87] E. Courvoisier, P.A. Williams, G. K. Lim, C.E. Hughes, K.D.M. Harris, CCDC 855058:
890 Experimental Crystal Structure Determination, 2014, doi: 10.5517/ccxprjv
- 891 [88] M. Woinska, S. Grabowsky, P.M. Dominiak, K. Woźniak, D. Jayatilaka, CCDC 1423912:
892 Experimental Crystal Structure Determination, 2016, doi: 10.5517/ccdc.csd.cc1jspnn
- 893 [89] F.R. Fronczek, H.N. Kamel, M. Slattery, CCDC 224658: Experimental Crystal Structure
894 Determination, 2014, doi: 10.5517/cc7js1k

- 895 [90] F.R.Fronczek, H.N. Kamel, M. Slattery CCDC 224659: Experimental Crystal Structure
896 Determination, 2014, DOI: 10.5517/cc7js2l
- 897 [91] E. Courvoisier, P.A. Williams, G.K. Lim, C.E. Hughes, K.D.M. Harris, The crystal structure of
898 L-arginine, *Chem. Commun.* 48 (2012) 2761-2763. doi: 10.1039/c2cc17203h.
- 899 [92] M. Woinska, S. Grabowsky, P.M. Dominiak, K. Wozniak, D. Jayatilaka, Hydrogen atoms can
900 be located accurately and precisely by x-ray crystallography, *Sci. Adv.* 2 (2016). doi:
901 10.1126/sciadv.1600192.
- 902 [93] F.R. Fronczek, H.N. Kamel, M. Slattery, Three polymorphs (alpha, beta and delta) of D-
903 mannitol at 100 K, *Acta Crystallogr. C* 59 (2003) 567-560. doi: 10.1107/S0108270103018961.
- 904 [94] P.J. Cox, P.L. Manson, CCDC 217467: Experimental Crystal Structure Determination, 2014,
905 doi: 10.5517/cc7992w
- 906 [95] K. Ostrowska, M. Kropidłowska, A. Katrusiak, CCDC 1041383: Experimental Crystal
907 Structure Determination, 2015, doi: 10.5517/cc13yn0q
- 908 [96] P.J. Cox, P.L. Manson, gamma-indomethacin at 120 K, *Acta Crystallogr. Sect. E Struct. Rep*
909 *Online* 59 (2003) 986-988. doi: 10.1107/S160053680301290X
- 910 [97] K. Ostrowska, M. Kropidłowska, A. Katrusiak, High-Pressure Crystallization and Structural
911 Transformations in Compressed R,S-Ibuprofen, *Cryst. Growth Des.* 15 (2015) 1512-1517. doi:
912 10.1021/cg5018888.
- 913 [98] S.A. Surwase, J.P. Boetker, D. Saville, B.J. Boyd, K.C. Gordon, L. Peltonen, C.J. Strachan,
914 Indomethacin: New Polymorphs of an Old Drug, *Mol. Pharm.* 10 (2013) 4472-4480. doi:
915 10.1021/mp400299a.
- 916 [99] M.L. Vueba, M.E. Pina, De Carvalho, L A E Batista, Conformational stability of ibuprofen:
917 Assessed by DFT calculations and optical vibrational spectroscopy, *J. Pharm. Sci.* 97 (2008) 845-
918 859. doi: 10.1002/jps.21007.
- 919 [100] J. Breitenbach, W. Schrof, J. Neumann, Confocal Raman-spectroscopy: Analytical approach
920 to solid dispersions and mapping of drugs, *Pharm. Res.* 16 (1999) 1109-1113. doi:
921 10.1023/A:1018956304595.
- 922 [101] L.S. Taylor, F.W. Langkilde, G. Zografi, Fourier transform Raman spectroscopic study of the
923 interaction of water vapor with amorphous polymers, *J. Pharm. Sci.* 90 (2001) 888-901. doi:
924 10.1002/jps.1041.
- 925 [102] S.L. Wunder, M.I. Bell, G. Zerbi, Band Broadening of CH₂ Vibrations in the Raman-Spectra
926 of Polymethylene Chains, *J. Chem. Phys.* 85 (1986) 3827-3839. doi: 10.1063/1.450903.
- 927 [103] J. Barra, F. Falson-Rieg, E. Doelker, Influence of the organization of binary mixes on their
928 compactibility, *Pharm. Res.* 16 (1999) 1449-1455. doi: 10.1023/A:1018967529128.

929 [104] M.N. Slipchenko, H. Chen, D.R. Ely, Y. Jung, M.T. Carvajal, J. Cheng, Vibrational imaging
 930 of tablets by epi-detected stimulated Raman scattering microscopy, *Analyst* 135 (2010) 2613-2619.
 931 doi: 10.1039/c0an00252f.

932 LIST OF FIGURES AND TABLES

933 Tables

934 **Table 1.** The compositions of different tablet formulations determined by DoE.

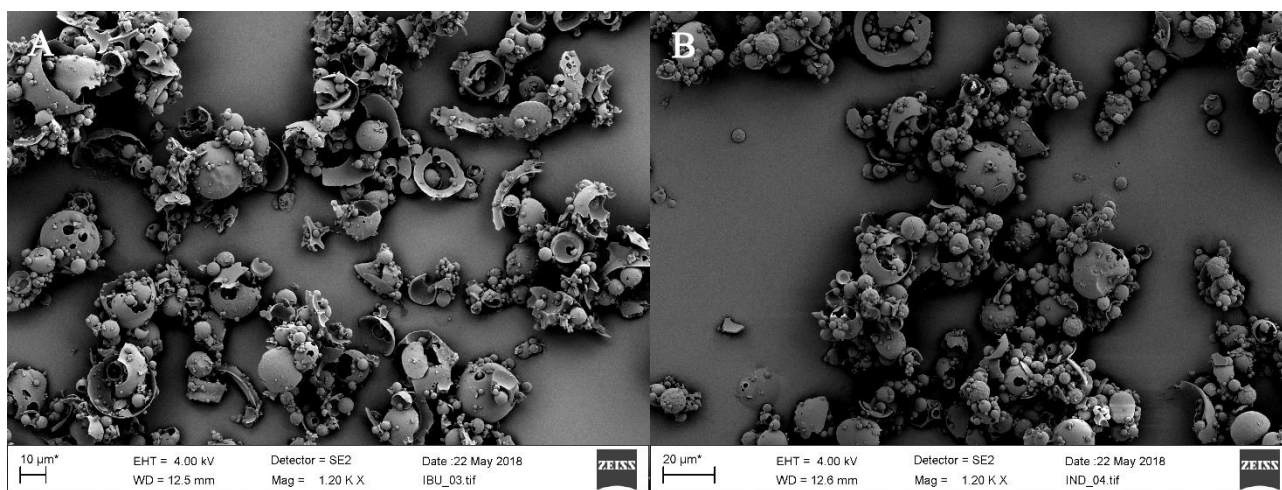
Tablet identifier	Amount of IBU-ARG (amount of IBU)	Amount of PVP	Sugar alcohol*	Tablet mass
B1	92.2 mg (50 mg)	30.7 mg	Xylitol	307.3 mg
B2	138.3 mg (75 mg)	30.7 mg	Xylitol	422.5 mg
B3	92.2 mg (50 mg)	30.7 mg	Mannitol	307.3 mg
B4	138.3 mg (75 mg)	30.7 mg	Mannitol	422.5 mg
B5	92.2 mg (50 mg)	46.1 mg	Xylitol	345.8 mg
B6	138.33 mg (75 mg)	46.1 mg	Xylitol	461.1 mg
B7	92.2 mg (50 mg)	46.1 mg	Mannitol	345.8 mg
B8	138.33 mg (75 mg)	46.1 mg	Mannitol	461.1 mg
B9	115.3 mg (62.5 mg)	38.4 mg	Xylitol	384.3 mg

Tablet identifier	Amount of IND-ARG (amount of IND)	Amount of PVP	Sugar alcohol*	Tablet mass
N1	74.3 mg (50 mg)	24.8 mg	Mannitol	247.8 mg
N2	111.5 mg (75 mg)	24.8 mg	Mannitol	340.8 mg
N3	74.3 mg (50 mg)	38.5 mg	Mannitol	282.0 mg
N4	111.5 mg (75 mg)	38.5 mg	Mannitol	375.0 mg
N5	74.3 mg (50 mg)	24.8 mg	Xylitol	247.8 mg
N6	111.5 mg (75 mg)	24.8 mg	Xylitol	340.8 mg
N7	74.3 mg (50 mg)	38.5 mg	Xylitol	282.0 mg
N8	111.5 mg (75 mg)	38.5 mg	Xylitol	375.0 mg
N9	92.9 mg (62.5 mg)	31.65 mg	Mannitol	311.4 mg

*Neither mannitol or xylitol have been shown to undertake Maillard reactions [39]

935

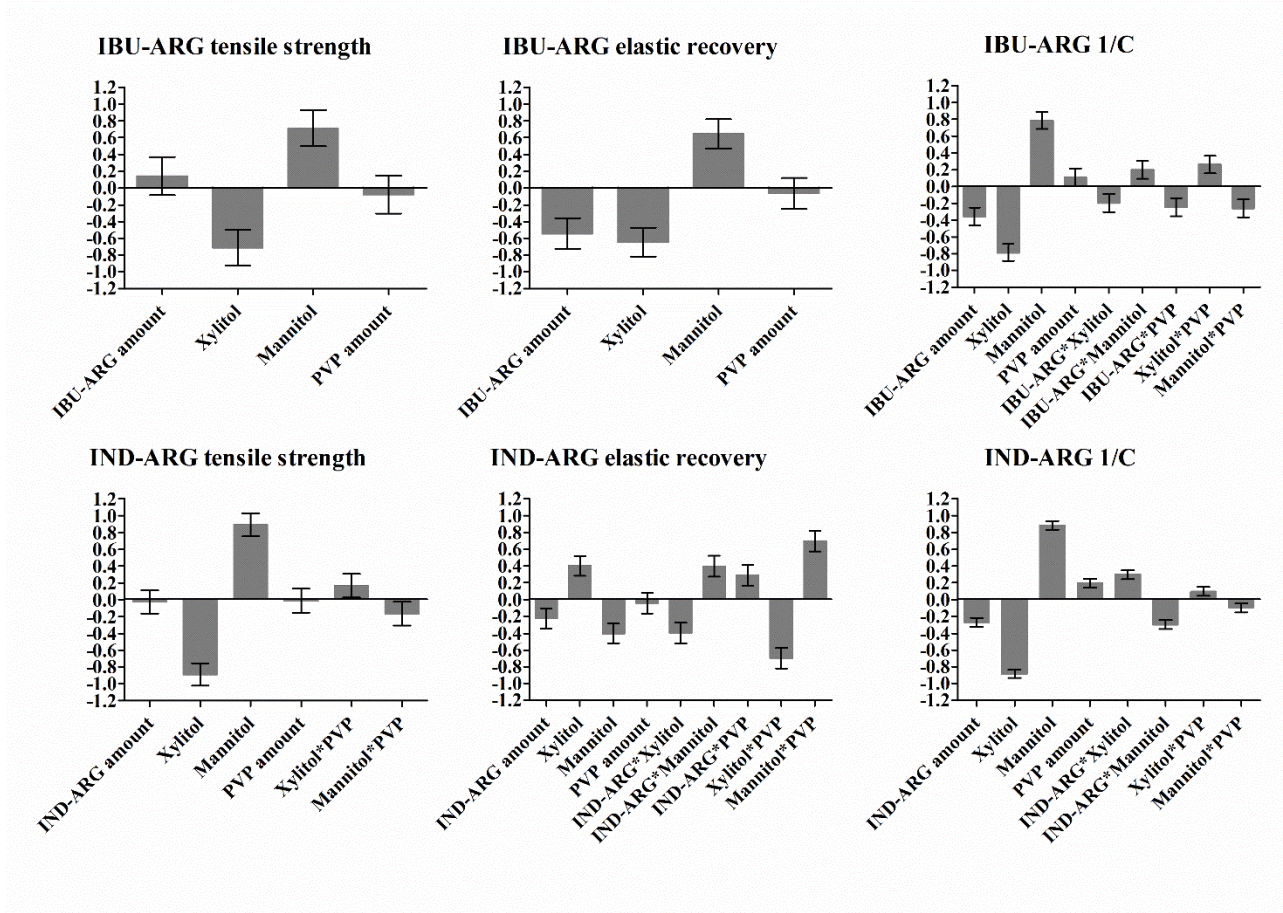
936 Figures



937

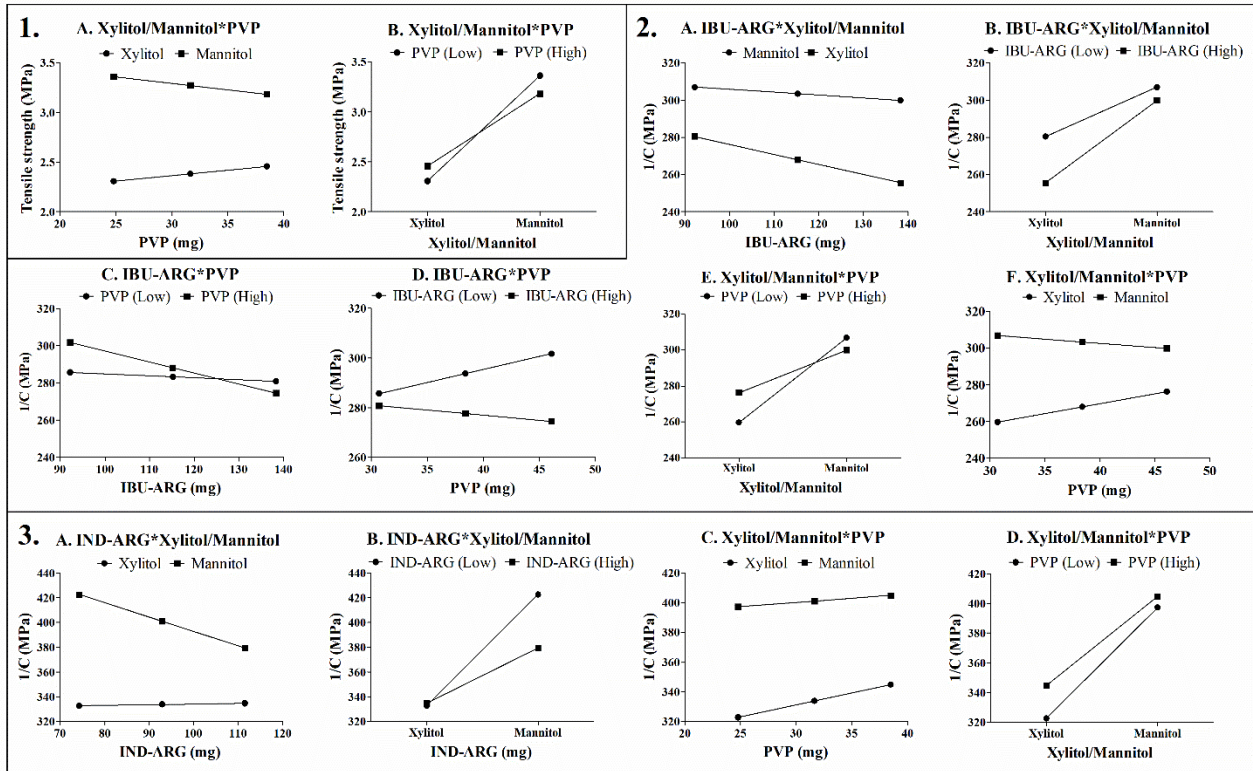
938 **Fig. 1.** Scanning electron microscope images of the spray dried ibuprofen-arginine (A) and

939 indomethacin-arginine (B) mixtures.



940

941 **Fig. 2.** The normalized coefficient plots of the models describing the effect of the amount of co-
 942 amorphous ibuprofen-arginine (IBU-ARG) or indomethacin-arginine (IND-ARG) salt, the amount
 943 of PVP and the sugar alcohol species (mannitol OR xylitol) on the mechanical properties of the
 944 tablets.



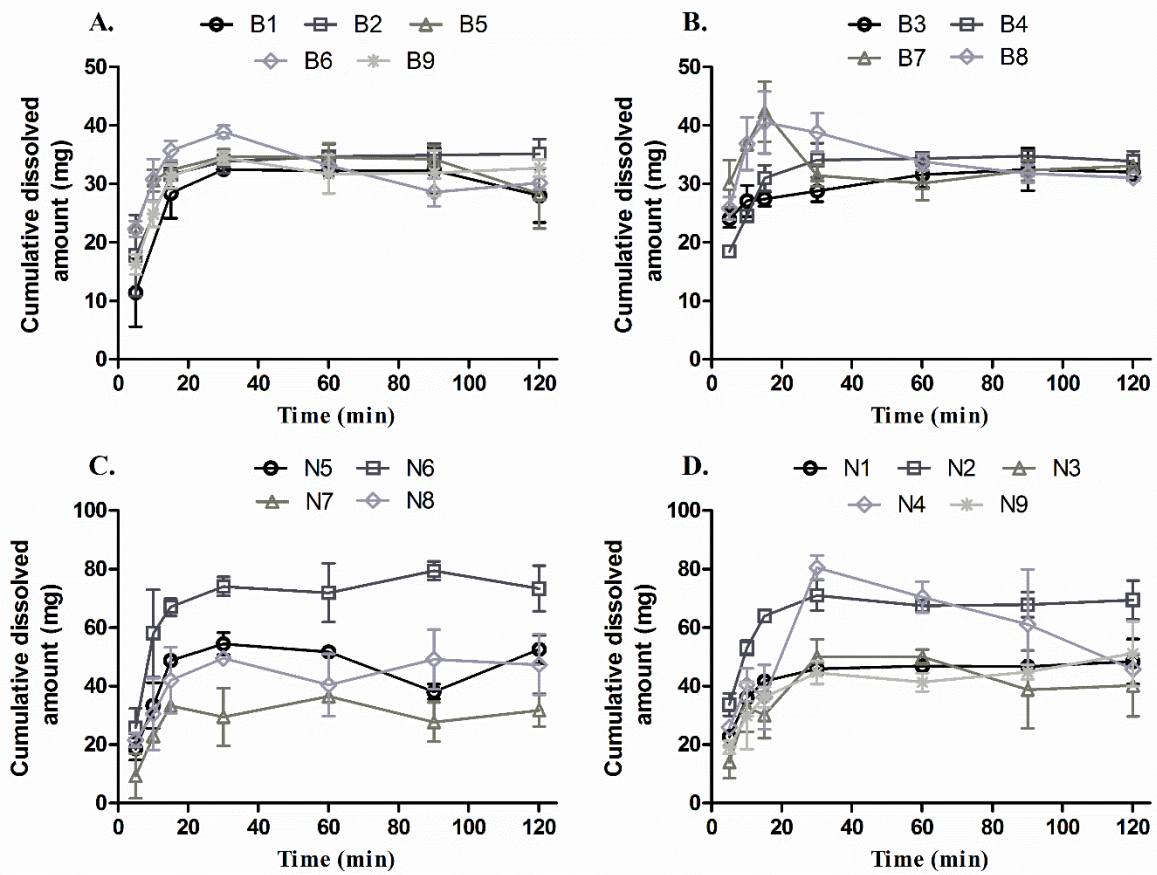
945

946

947

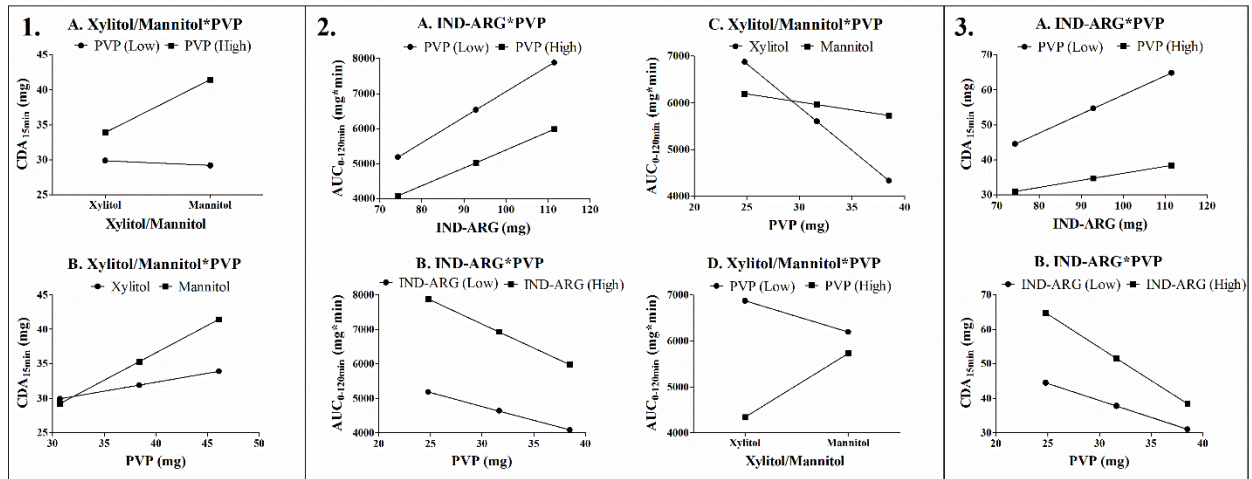
948

Fig. 3. The interaction plots of models describing the effect of changes in tablet composition on the tensile strength of N formulations (1.) as well as on the 1/C value of B formulations (2.) and N formulations (3.).



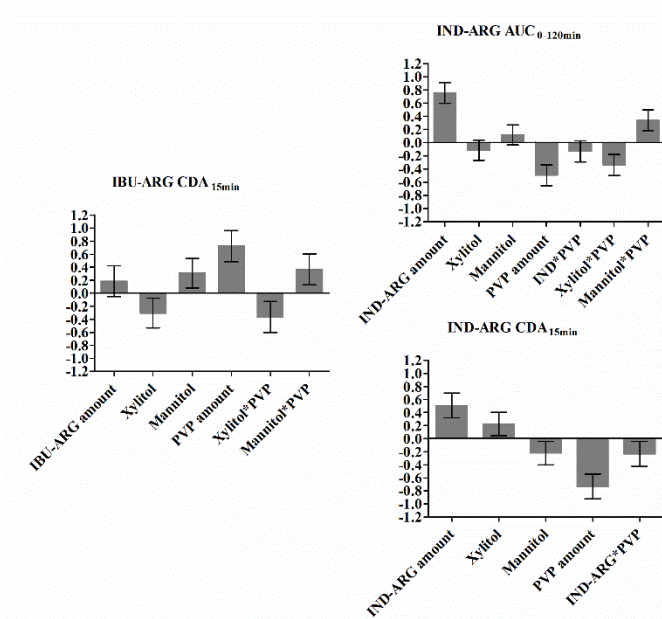
949

950 **Fig. 4.** Dissolution profiles of A. IBU-ARG and xylitol containing tablets in pH 1.2, B. IBU-ARG
 951 and mannitol containing tablets in pH 1.2, C. IND-ARG and xylitol containing tablets in pH 5.0 and
 952 D. IND-ARG and mannitol containing tablets in pH 5.0. The drug doses in different formulations
 953 were 50 mg (B1, B3, B5, B7, N1, N3, N5, N7), 62.5 mg (B9, N9) or 75 mg (B2, B4, B6, B8, N2,
 954 N4, N6, N8).



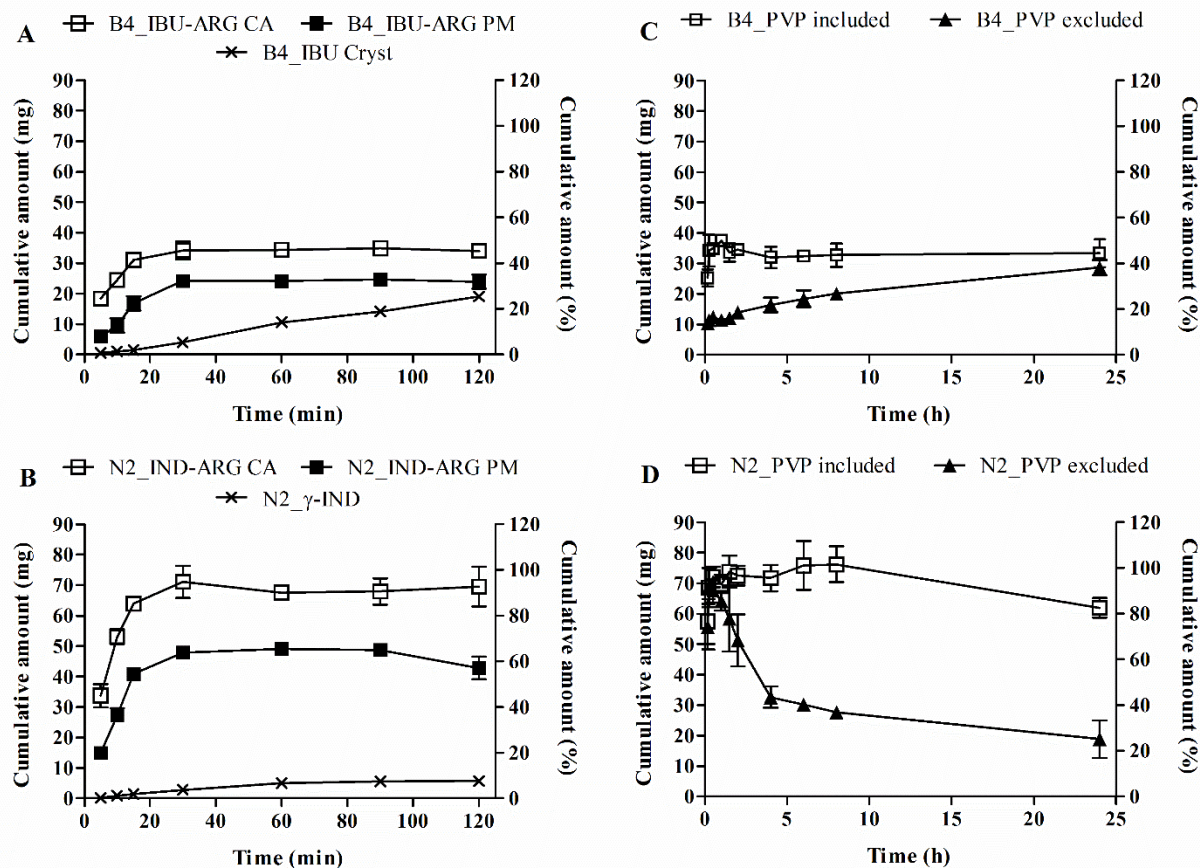
955

956 **Fig. 5.** The interaction plots of models predicting the effect of the tablet composition on the
 957 CDA_{15min} of B formulations (1.) as well as on the AUC_{0-120min} (2.) and CDA_{15min} (3.) of N
 958 formulations.



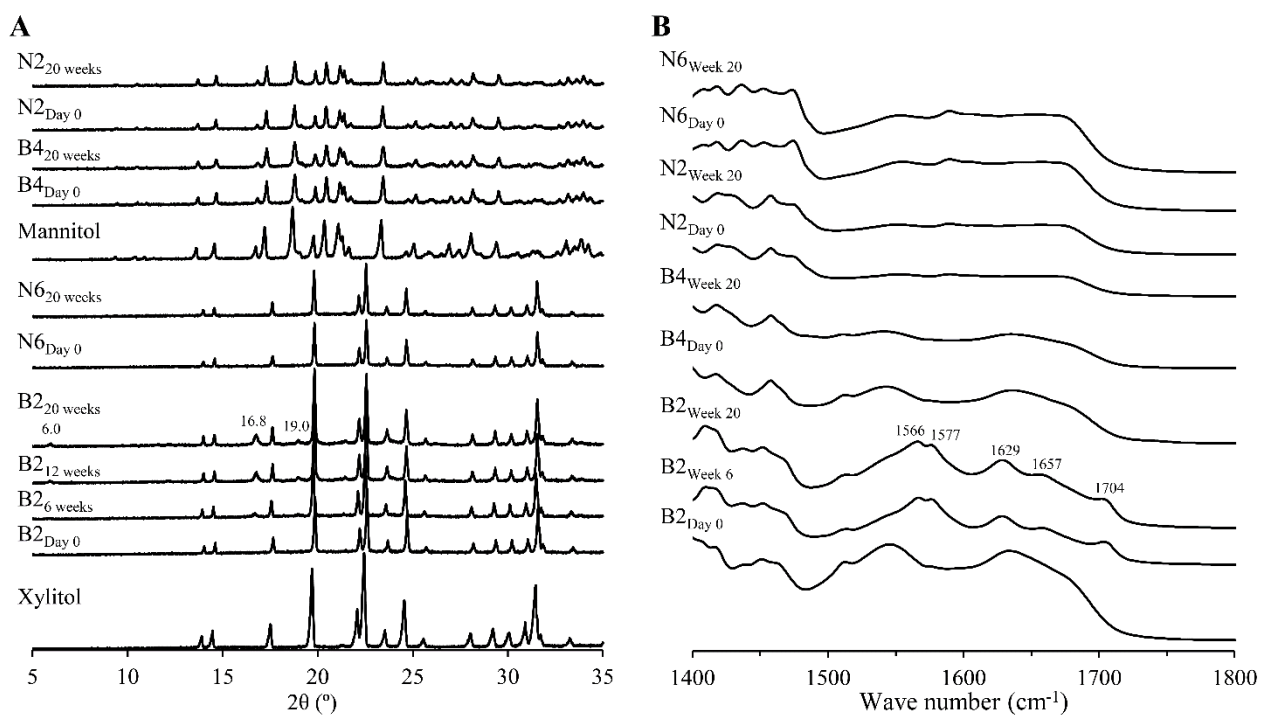
959

960 **Fig. 6.** The normalized coefficient plots of the models describing the effect of the amount of co-
 961 amorphous ibuprofen-arginine (IBU-ARG) or indomethacin-arginine (IND-ARG) salt, the amount
 962 of PVP and the sugar alcohol species (mannitol or xylitol) on the area under the cumulative
 963 dissolved drug amount-time curve between 0 and 120 minutes (AUC_{0-120min}) and on the
 964 cumulative dissolved drug amount after 15 minutes (CDA_{15min}).



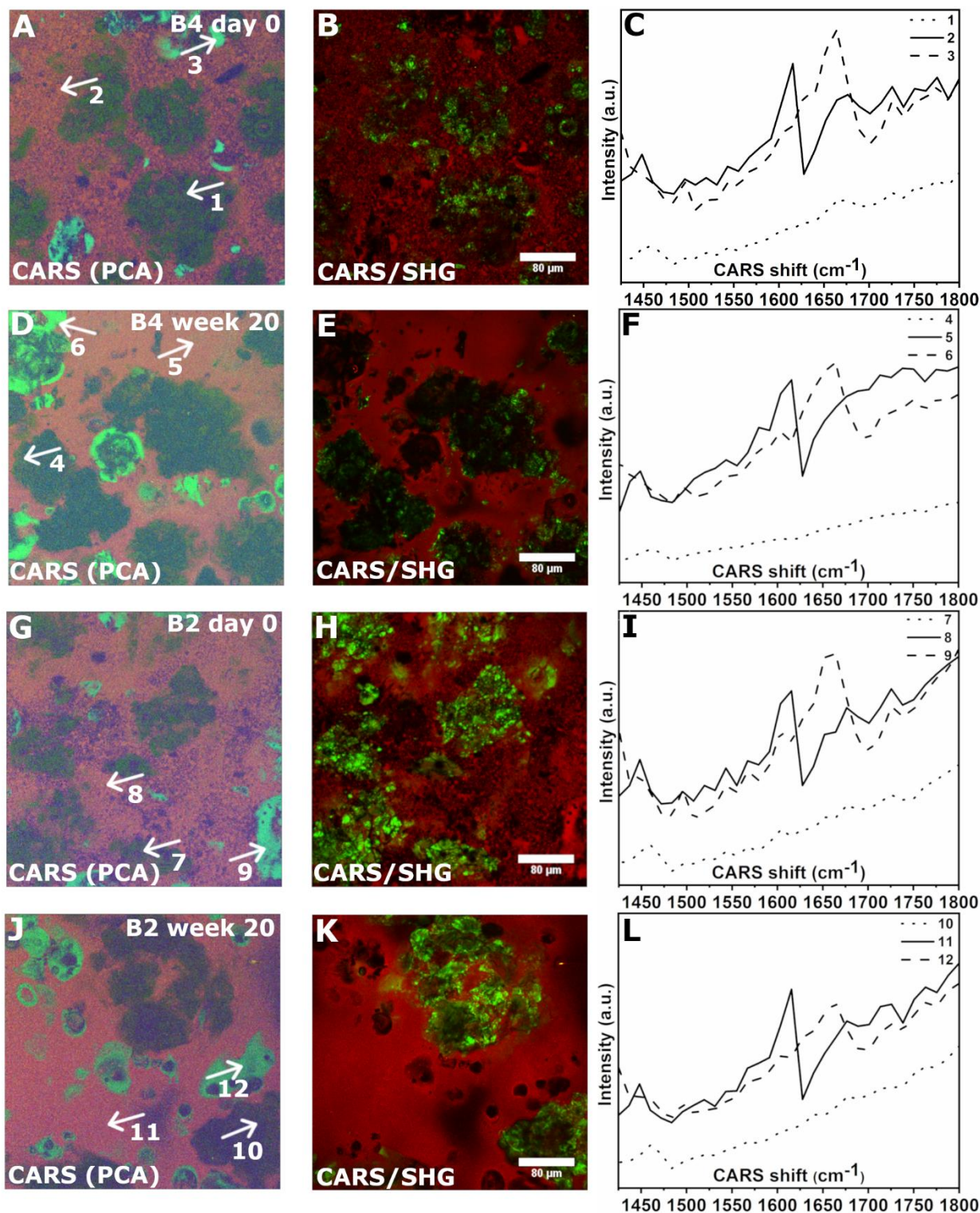
965

966 **Fig. 7.** The investigation of the effect of arginine (ARG) and the formation of co-amorphous salt
 967 (CA) on the release of ibuprofen (IBU) and indomethacin (IND) from B4- and N2-formulations (A
 968 and B, respectively) as well as the effect of polyvinylpyrrolidone K30 (PVP) on the supersaturation
 969 stability after drug release from B4- and N2-formulations (C and D, respectively). PM denotes
 970 physical mixture and Cryst crystalline drug.



971

972 **Fig. 8.** The X-ray diffractograms (A) and FTIR spectra (B) of B2-, B4-, N2- and N6-formulations at
 973 day 0 and after storage under ambient temperature and 33% relative humidity. With formulations
 974 that showed no signs of recrystallization, only the data from the beginning and end of the study are
 975 shown, but with B2 formulation the data from several time points is included. The diffractograms of
 976 mannitol and xylitol are also included for comparison.



977

978 **Fig. 9.** The PCA based CARS images of tablet surfaces of B4- and B2- formulations (left column,
 979 A,D,G,J), corresponding the overlaid CARS/SFG/SHG images (at 1652 cm^{-1}) (middle column,
 980 B,E,H,K) and CARS spectra extracted from regions marked with white arrows and numbers (right
 981 column, C,F,I,L) on day 0 and on week 20. The PCA RGB image is generated from a CARS

982 spectral scan in the region $1417\text{--}1804\text{ cm}^{-1}$, using the score values of the first three PCs. PCA
983 loadings are shown in Figure S8. The scale bar is $80\text{ }\mu\text{m}$.